 doi:10.20944/preprints202210.0090.v1

Article

Transformational Geothermal Fluids in the Upper Jurassic Carbonate Reservoir of the South German Molasse Basin

Jochen Schneider [1,*], Florian Heine [2,3], Michael Heidinger [3] and Martin Rosner [4]

[1] Hydrosion GmbH, Tizianstr. 96, 80638 Munich, Germany; jochen.schneider@hydrosion.de
[2] Chair of Hydrogeology, Department of Civil, Geo and Environmental Engineering, Technical University of Munich, Arcisstr. 21, 80333 Munich, Germany; florian.heine@tum.de
[3] Hydroisotop GmbH, Woelkestr. 9, 85301 Schweitenkirchen, Germany; mh@hydroisotop.de
[4] Isoanalysis UG, Volmerstr.7, 12489 Berlin, Germany; martin.rosner@isoanalysis.de
* Correspondence: Jochen.Schneider@hydrosion.de;

Abstract: The hydrochemical composition of the Upper Jurassic groundwaters in the South German Molasse Basin (SGMB) indicates a heterogeneous and varying hydrogeochemical evolution, which contradicts previous flow model concepts. For this study, the data of 88 Tertiary, Cretaceous and Upper Jurassic groundwater samples were investigated for hydrochemical elements, $^{2}H/^{18}O$-H_2O isotopes, $^{87}Sr/^{86}Sr$ ratios as well as $\delta^{11}B$ values. In addition, the geochemical composition, $^{87}Sr/^{86}Sr$ and $\delta^{11}B$ values were analysed from depth-oriented Upper Jurassic rock samples to delineate water-rock interactions in the aquifer systems. Slightly elevated $^{87}Sr/^{86}Sr$ ratios of the carbonates compared to the typical signatures of marine Upper Jurassic carbonates indicate a synsedimentary radiogenic influence due to the erosion of the adjacent Bohemian Massif. However, these values cannot explain the significant higher Sr-isotope fingerprint of the groundwaters in the central SGMB. Different water types occur in the Upper Jurassic aquifer, primarily distinguished by the dominant cations, calcium or sodium with subclasses of the major anions. The calcium-dominated groundwaters occur mainly at the western and northern margins of the SGMB. The sodium-dominated ion exchange groundwaters instead dominate in the central and eastern SGMB. With increasing strontium content, the $^{87}Sr/^{86}Sr$ ratios of the Upper Jurassic groundwater samples either indicate a strontium uptake by carbonate of the host rocks, or a prevailing radiogenic signature. This implies a basic interaction with terrestrial or marine Tertiary sediments. The results illustrate a downward transformational fluid flow systematic via the thick Tertiary sediment cover into the Upper Jurassic carbonate formation in the SGMB, highlighting a new understanding on the evolution of the Upper Jurassic groundwaters and a basin-wide recharge mechanism.

Keywords: Environmental isotope analyses; Strontium isotopes; Boron isotopes; Upper Jurassic carbonate aquifer; South German Molasse Basin; Tansformational Fluid Flow; Geothermal

1. Introduction

The Upper Jurassic aquifer in the South German Molasse Basin (SGMB) represents an intensively used reservoir for many purposes such as drinking water production in shallow parts of the basin as well as balneological and geothermal applications in greater depths. At the beginning of 2021, there are 23 geothermal plants operating with thermal water from the Upper Jurassic carbonate aquifer to generate heat, electricity and combined heat and electricity [1]. For geothermal heat extraction and electricity generation, especially the central area of the SGMB plays a major role in Germany. The central SGMB includes the city of Munich and surrounding communities as well as areas in the southeast of Bavaria towards the Alps and the Austrian border.

Regional flow systems and the hydrochemical characteristics of the groundwater in the Upper Jurassic carbonates have already been described since the 1950s [2–13]. In the

 doi:10.20944/preprints202210.0090.v1

course of further exploration and accompanying research during the last decades, the concept of a large-scale flow system covering the entire Molasse Basin was described and continuously adapted with hydraulic and hydrochemical data from subsequently drilled geothermal wells until 2014 [5,11,13–16]. The studies postulate recharge and partly discharge areas in the west and north of the SGMB, in the exposed Swabian Alb and Franconian Alb and a general groundwater flow from west to east towards the central SGMB. However, these earlier studies were conducted without the knowledge of the groundwater composition of the recently developed geothermal plants and drilled wells.

Several types of groundwaters and different individual hydrochemical zones were distinguished based on elemental groundwater analyses in the Upper Jurassic aquifer of the SGMB by various authors [8,9,13,17,18]. Thereby, the Upper Jurassic groundwaters were described as very heterogeneous with a wide range of water types from recently formed low mineralised Ca-(Mg)-HCO_3 waters in the northern and western parts of the reservoir to higher mineralised Na-Cl waters in the southwestern SGMB. In addition, the stable water isotope signatures of the groundwaters indicate different climatic conditions during recharge and partly intensive water-rock interaction with the reservoir rocks or influences of highly saline formation or oilfield waters [4,13,19].

However, the interpretation of present hydraulic potential and the delineated general flow system of today seem to contradict the previously postulated hydrogeochemical genesis and evolution of the Upper Jurassic groundwaters [13,15,17,20]. Moreover, the recharge areas of the geothermally used groundwaters occurring in the central SGMB are yet not fully understood.

Besides well-established hydrochemical tracers like major and trace elements or environmental isotope methods such as $^{2}H/^{18}O$-H_2O, the $^{87}Sr/^{86}Sr$ ratio of dissolved strontium is a very suitable tracer for characterising the maturation of groundwater by water-rock interaction. This isotope method has been applied successfully in various hydrogeological studies [21–28]. Based on analyses of fossils and whole rock samples of marine carbonates, the Phanerozoic evolution of the $^{87}Sr/^{86}Sr$ ratio in seawater was reconstructed [29–31]. The resulting Phanerozoic $^{87}Sr/^{86}Sr$-seawater curve is linked to the global endogenic and exogenic processes through time [31]. Pre-assessment of $^{87}Sr/^{86}Sr$ signatures of geothermal waters from the Upper Jurassic aquifer of the SGMB showed more radiogenic values [32,33] than typically expected for Upper Jurassic marine carbonates [34].

Based on the contradiction in the hydrogeological systematic of Upper Jurassic groundwater in the SGMB and the pre-assessment of $^{87}Sr/^{86}Sr$ signatures obtained from several projects and regional studies [18,32,33,35,36], the aim of this comprehensive study is to characterise the Upper Jurassic groundwaters in the SGMB as well as the host rocks.

For this purpose, the scientific IsoMol project was initiated by the Bavarian Environmental Agency (LfU) and the Technical University Munich (Chair of Hydrogeology). Within this framework, hydrochemical and environmental isotope analyses were performed on groundwater ($\delta^{18}O$/ $\delta^{2}H$ values, $^{87}Sr/^{86}Sr$ ratios) from aquifers within the SGMB and rock ($^{87}Sr/^{86}Sr$) samples from the Upper Jurassic carbonates in the SGMB. The objective is to evaluate the results in a large-scale study with systematic analyses and comparison of rock and water samples.

For an improved understanding of the geothermal system in the SGMB, a small set of water and rock samples were also analysed for their $\delta^{11}B$ values. Thereby, the use of the boron isotopic composition in a geothermal context represents a rather new approach. However, due to the large natural variation of $\delta^{11}B$ and isotope fractionation, $\delta^{11}B$ values enable the investigation of mixing and water-rock interaction processes in groundwater [37–39].

This study presents the results of recently obtained hydrochemical and isotope data of rock and water samples [18,40] and is supported by data from the project "Dolomitkluft" [36] and the Interreg IIIA study [33], which was partly published in the NAGRA-Report [33,35]. In addition, selected vein calcite samples were analysed regarding $\delta^{13}C$/ $\delta^{18}O$-$CaCO_3$ values to establish relations to extensive preliminary investigations [41].

 doi:10.20944/preprints202210.0090.v1

2. Description of the study area

The study area SGMB is part of the Cenozoic foreland basin in the north of the Alps. The basin extends from eastern France via Switzerland and Germany to Austria with a length up to 1,000 km and was formed as a consequence of the Alpine orogeny.

The SGMB comprises the federal states of Bavaria and Baden-Wuerttemberg in southern Germany. It is bounded in the north and west by the outcropping Upper Jurassic carbonates of the Franconian Alb and Swabian Alb, in the south by the Alps and in the east by the crystalline basement rocks of the Bohemian Massif [42,43].

2.1. Geologic description of the SGMB

The basin filling of the SGMB mainly consists of Tertiary sediments, which fundamentally responded to flexural subsidence. The sequence covers the southward dipping sedimentary rocks (**Figure 1**) of the Cretaceous and Jurassic [42]. The filling contains shallow marine and continental-fluviatile sedimentary rock sequences originating from erosional processes of the uprising Alps and crystalline/metamorphic basement rocks of the Bohemian Massif in the vicinity of the SGMB [42,43]. These sediments overstep the Variscan basement and are divided by the "Landshut-Neuoetting High" (LNH), a Variscan SW-NE trending basement ridge into the so-called "Braunauer Trog" east of the LNH and "Wasserburger Trog" between the LNH and Munich [42,43].

The sequences of sandstones, mudstones and marine and freshwater carbonates are deposited either fluviatile (OSM: Upper Freshwater Molasse and USM: Lower Freshwater Molasse) or shallow marine (OMM: Upper Marine Molasse and UMM: Lower Marine Molasse) during Neogene and Paleogene [42,43]. The western and northern rather shallow parts of the Molasse Basin show a widespread heterogenous Tertiary overlay directly on the Upper Jurassic carbonates. Following, it may be assumed, that the terrigenous sediments are partly in hydraulic contact with the Upper Jurassic aquifer system in this area [44].

During Cretaceous the Tethys transgressed and regressed, causing erosional phases with subaerial exposure, dissolution, dolomitization and initial karstification of the underlying Upper Jurassic carbonates by meteoric waters [45–47]. The Cretaceous sediments consist predominantly of marine carbonate rocks with marls and limestones and cover the Upper Jurassic carbonates only in the eastern and south-eastern central basin. The lowermost Cretaceous sediments overlying the Upper Jurassic carbonates are the evaporitic Purbeckian, which primarily consist of shallow water carbonates and marls [48].

The marine realm of the Tethys developed in the Upper Jurassic in southern Germany to an epicontinental shallow marine shelf environment. Here, marine limestones and dolostones were sedimented, surrounded by the emerging Bohemian massif in the east and north. Within the SGMB, the Upper Jurassic rocks can be divided in three main facies: the Swabian facies with higher proportions of marly carbonates in the western SGMB; the Franconian facies with characteristic reef platforms and overall lower proportions of marly carbonates in the eastern SGMB; and the dense and bitumen-rich, so-called Helvetican facies in the southwestern SGMB [51,52].

The sedimentation area of the Franconian and Swabian facies can be roughly subdivided along a lineament, today visible by the river Lech [52]. These main facies can further be subdivided in sedimentation environments of massive (reef) or bedded facies with different lithologic and hydraulic characteristics [51].

The Upper Jurassic carbonate platform has a thickness of approximately 400 to 600 m and dips from the exposed Swabian and Franconian Alb towards the south. As a hydrogeothermal reservoir, the carbonate platform encounters depths up to 2,000 m in the north of Munich and over 5,000 m at the fringe of the Alps [43,50]. Thus, the reservoir temperatures increase from north to south and can reach up to 160 °C [1].

The Upper Jurassic reservoir rocks show a wide range of matrix porosities (>1 % to 20 %) and hydraulic permeabilities (10^{-4} to 10^{2} mD) [53–57]. The Upper Jurassic aquifer is

Preprints (www.preprints.org) | NOT PEER-REVIEWED | Posted: 8 October 2022 doi:10.20944/preprints202210.0090.v1

represented mainly by dolomitised and highly permeable carbonates of the Kimmeridgian and Tithonian stage which also incorporate karstic features [46,50]. Underlying Oxfordian rock sequences generally demonstrate low permeability. Due to multiple factors and parameters, such as stress field propagation, tectonics and rock facies, the hydraulic permeability in the south of the SGMB and south-west of Munich is several magnitudes lower than in the northern part of the basin [16,41,53–55].

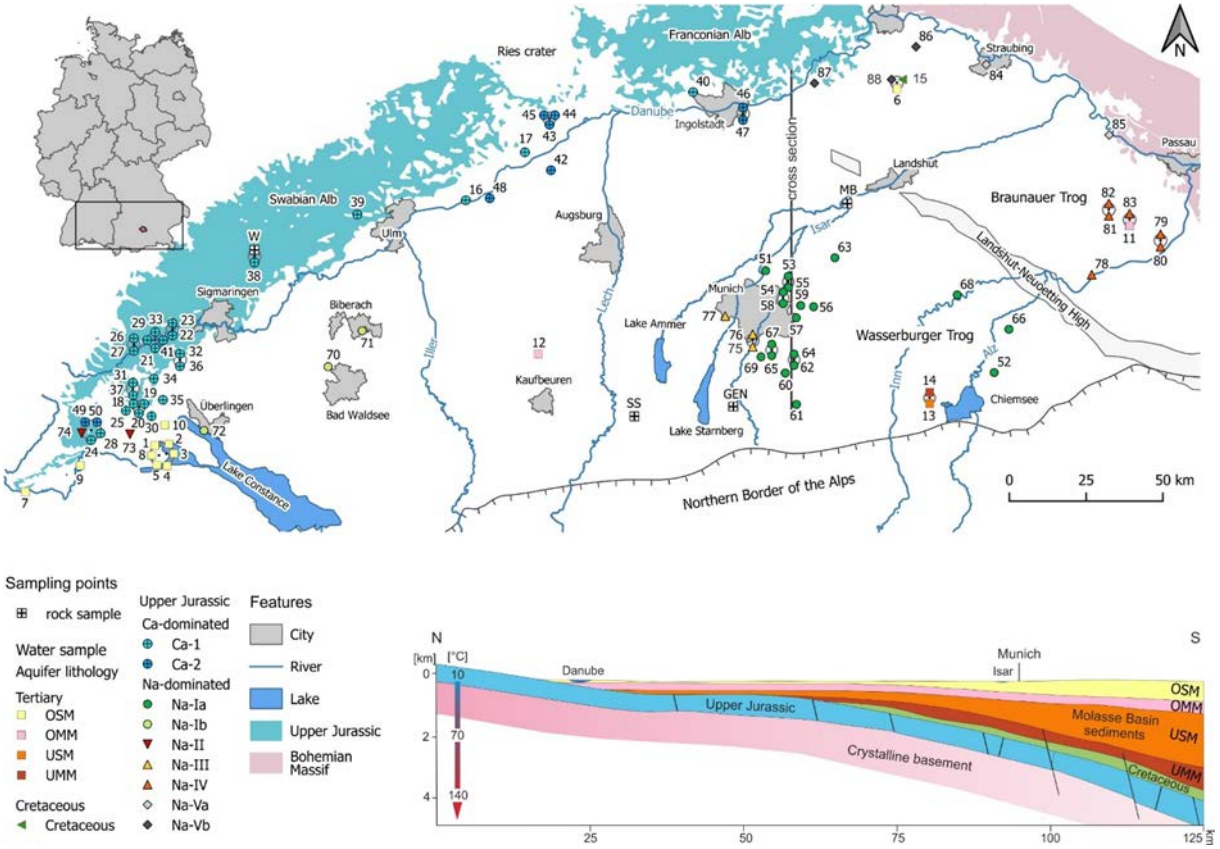

Figure 1: Overview of the study area in Southern Germany with sampling locations, geographical terms, and geological features. Geological schematic cross section through the Bavarian Molasse basin showing the Upper Jurassic sediments dipping in a southward direction (modified after [49,50]).

2.2. Hydrogeological situation of the Upper Jurassic aquifer

The regional groundwater flow system of the Upper Jurassic aquifer has already been described and discussed in several previous studies (e.g. [6,11,12,15,16,46,58,59]). The perspectives on groundwater recharge and flow characteristics were developed from general assumptions based on outcrops of the Upper Jurassic rocks, the geometry of the SGMB and the Danube drainage system on its northern boundary. This resulted in the hypothesis of a combination of inflow from northern boundaries and recharge in defined areas north to the Lake Constance with assessed high groundwater levels [6,11,15]. The hydraulic potential analyses further indicated a general flow direction parallel to the discharging river Danube from the western SGMB to the LNH in the east with recharge areas in the Swabian Alb in Baden-Wuerttemberg [11,46]. In the north-east of the LNH, recharge was described to occur in the Franconian Alb nearby the city of Regensburg with a general south-eastern flow direction towards the Braunauer Trog [11]. Deep groundwaters from the SGMB, to the west of the LNH, were assumed to flow northwards and drain into the river Danube in some areas nearby the city of Ulm as well as between the cities Ingolstadt and Regensburg [8,9]. However, the Upper Jurassic flow system, especially within greater depths in the SGMB, is yet controversially discussed due to an approach by Savvatis et al. [58]. In

 doi:10.20944/preprints202210.0090.v1

contrast to the interpretation of the hydraulic potentials, the water chemistry and isotope data of the Upper Jurassic groundwaters may suggest a deviating picture of the hydraulic system, particularly based on distinct hydrochemical provinces in the western, central, eastern, and northern SGMB [13].

In the central SGMB near Munich (**Figure 1**), the occurring groundwaters were mostly classified as Na-[Ca]-HCO_3-Cl waters with a low mineralisation (up to 800 mg/l) and showed a typical ion exchange character between calcium and sodium [4,7,10,12,13]. The groundwaters were formed under predominantly cold climatic conditions based on the stable water isotope values [9,10,13], derived noble gas infiltration temperatures between 0.9 and 3.1 °C [9,18] and ^{81}Kr model ages between 60,000 and 135,000 years [60]. Towards the western central SGMB, higher mineralised waters of the Na-Cl type occur, which were formed under different recharge conditions. They show substantial water-rock interactions which could be traced back to mixing with highly saline fossil formation or oilfield waters [6,13,18,46].

The majority of shallow groundwaters at the western and northern margin of the SGMB are mostly of the Ca-[Mg]-HCO_3 type and were recharged under predominantly warm climate conditions [8,9,44]. Generally, they include considerable amounts of tritium and radiocarbon (DIC) which indicate modern, sub-modern and medium old groundwater ages [9,35,44,61,62]. Some groundwaters in the proximity of the river Danube, especially to the north-east of the basin, deviated from this and show similar hydrochemical characteristics to groundwaters from the central SGMB.

To the north of Lake Constance in the western SGMB, it is assumed that the occurring ion-exchange waters of mostly Na-HCO_3 type were recharged under high pressure during glacial periods in pronounced subglacial environments [10,12]. They have been infiltrated via transformational flow, which has been recently highlighted by ^{81}Kr model ages [60] and newly obtained radiocarbon age analyses in dissolved organic carbon (DOC) [44].

The Upper Jurassic waters occurring in the Braunauer Trog in the eastern SGMB are geologically separated from the waters in the central SGMB by the crystalline LNH, which act as a natural hydraulic barrier [3]. These ion-exchange waters show an almost completed geochemical alteration, low contents of earth-alkaline metals and a Na-HCO3-Cl dominated signature. [11,63]. ^{81}Kr age analyses from wells within that region as well as in the adjacent Upper Austria south of the Braunauer Trog with similar groundwaters [64,65], indicate apparent water ages between 500,000 and 565,000 years [60]. In the north-east of the Braunauer Trog and towards the outermost region of the basin, the influx of deep circulating crystalline waters along deep fault structures to the Upper Jurassic, is assumed to be responsible for higher mineralised Na-Cl-HCO_3 waters close to the city of Straubing and wells in the west [9,13].

3. Materials and analytical Methods

The objective of this study is to compare water samples from different wells and springs in the Upper Jurassic of the Bavarian Molasse Basin to some western regions considering the hydrochemical, hydrogen, oxygen, strontium and boron isotope composition with respect to their origin and genesis. Therefore, the easily accessible groundwaters of wells (**Figure 1**) from the succession of the Upper Jurassic to the Tertiary were sampled. Moreover, within this context rock samples from the Upper Jurassic aquifer were collected and analysed in various leaching steps to figure out water-rock exchange processes between the carbonates and the reservoir water.

3.1. Groundwater and rock sampling

A total of 20 carbonate samples and three calcite vein samples were collected from drilled rock cores from four different boreholes in the SGMB and the Swabian Alb (Figure 1) and are characterised in Table 1. In detail, these include:

Preprints (www.preprints.org) | NOT PEER-REVIEWED | Posted: 8 October 2022 doi:10.20944/preprints202210.0090.v1

- Five samples from the Moosburg well (MS) [66], which provide a complete profile of the Upper Jurassic sequence from the Tithonian to the Oxfordian at depths between 1,127 and 1,540 m TVD.
- One sample of Tithonian age, which was obtained from a very deep oil and gas well (SS) in the south-west of the central SGMB (4,300 m TVD).
- The Geretsried well, which was drilled for geothermal utilisation. However, also the second deviated well, where the rock material originates from, could not find enough water for an economic operation. A depth-resolved profile (4,595 to 4,710.9 m TVD) with ten rock samples (GS) of Upper Kimmeridgian age from the drill core from the second Geretsried borehole GEN-1ST-A1 as well as three vein calcite samples (GV) were analysed during the Dolomitkluft campaign [36].
- Four samples from the groundwater monitoring well Wilsingen (W), which were analysed in depths between 85 and 200 m TVD as part of the INTERREG IIIA campaign [33].

The rock and vein samples for all analyses were thoroughly cleaned with pure water and dried. Thereafter, the samples were crushed and milled to a fine-grained powder suitable to dissolve the rock powders in acid.

The locations of the 88 water samples collected from shallow wells, deep wells and springs from various aquifers are shown in Figure 1. A total of 73 water samples were obtained from the Upper Jurassic aquifer. They were sampled at springs and surface waters (4), drinking water wells (35), balneological and geothermal sites (34). In addition, 11 samples originate from wells tapping the Miocene Upper Freshwater Molasse (OSM), two from the Miocene Upper Marine Molasse (OMM), and one sample from the Miocene to Oligocene Lower Freshwater Molasse (USM) and Lower Marine Molasse (UMM), respectively.

The geothermal sites in Bavaria are part of the central SGMB nearby the city of Munich and the Wasserburger Trog in the east. Most of the investigated balneological sites are located to the east of the LNH in the Braunauer Trog and to the west of the SGMB in Baden-Wuerttemberg. The drinking water wells are located in proximity to the river Danube in the north and west of the SGMB.

All well samples were collected during the regular well operation and after the measurement and stabilisation of the physico-chemical parameters (pH-value, specific electrical conductivity (eC) and temperature) in a beaker. The samples of the geothermal wells were cooled to less than 70 °C. The sampling of the Upper Jurassic deep groundwater often resulted in degassing due to pressure release, which affected the measurement of in situ parameters, especially the pH and inorganic carbon species. The sampled water for laboratory measurements of the major ions, stable water isotopes as well as strontium and boron isotopes, was filled in either 30 ml HDPE or 50 ml LDPE bottles. They were partly stabilized (cation sample with 65 % HNO_3), cooled to 4 °C or frozen (anion samples) prior to the measurements.

3.2. Theoretical background of strontium and boron isotopes

Strontium comprises four stable isotopes (^{84}Sr, ^{86}Sr, ^{87}Sr, ^{88}Sr). In addition to its primordial abundance, only ^{87}Sr is formed radiogenically by radioactive decay from rubidium (^{87}Rb) with a half-life of ~4.88 x 10^{10} years [67]. Thereby, rubidium behaves as an incompatible element that crystallizes at the end of the magmatic series, substituting potassium in feldspars and micas. For that reason, acidic rocks such as granites and rhyolites are usually characterised by an increased content of rubidium. Carbonate rocks typically incorporate medium to low strontium contents. Strontium replaces calcium in Ca-bearing minerals such as calcite or dolomite. Due to the radioactive decay of ^{87}Rb to ^{87}Sr, high values of ^{87}Sr are typically found in old feldspars and mica-rich rocks. Therefore, rocks such as granites show considerably higher $^{87}Sr/^{86}Sr$ ratios ($^{87}Sr/^{86}Sr \geq 0.715$), while basalt is characterised by lower $^{87}Sr/^{86}Sr$ ratios of about 0.704 [29,34,67].

 doi:10.20944/preprints202210.0090.v1

Boron has two stable isotopes with a natural abundance of ^{11}B and ^{10}B of about 80 % and 20 %, respectively. In geo- and hydrochemistry, the boron isotope compositions are reported as $\delta^{11}B$ values relative to the certified reference material NIST SRM 951a. Boron is typically found in nature bound to oxygen. In water, dissolved boron occurs as $B(OH)_3$ and $B(OH)_4^-$ and the distribution of these species depends on the pH value of the water [37,68]. The boron concentrations in natural groundwaters tend to be lower than 0.5 mg/l, in open seawater approximately 4.5 mg/l and in fossil formation or fossil brines and oilfield waters up to 1380 mg/l [37,38].

In water, ^{10}B is preferably concentrated in $B(OH)_4$ and is often incorporated in carbonates. ^{11}B, on the other hand, is frequently enriched in $B(OH)_3$ and will remain in liquid phase [35]. The $\delta^{11}B$ value of modern seawater is about +40 ‰ [38]. In comparison to seawater, marine carbonates are characterised by lower $\delta^{11}B$ values (corals +20 ‰) [37]; foraminifera +13.3 ‰ [68]). Boron isotope studies on Late Cretaceous carbonates show $\delta^{11}B$ values less than +20 ‰ [68].

3.3. Analytical Methods

3.3.1. Physico-chemical parameters, major and trace ions

The physico-chemical parameters pH value, specific electrical conductivity (EC) and temperature (T) of the groundwater were determined with a set of WTW Multi 3430 sensors in the field. The pH value and EC are referred to a temperature of 25 °C. The titration of the carbonate species with 0.1 M HCl (HCO_3^-) and 0.01 M NaOH (CO_2) were also performed in the field.

The major ions (Ca^{2+}, Mg^{2+}, Na^+, K^+, Cl^-, SO_4^{2-}, F^-) of groundwater were analysed with an ion-chromatograph (Thermo Fisher ICS1100) at the Chair of Hydrogeology (TUM) and the trace elements (Sr^{2+}, Rb^+) were determined at the Institute of Water Chemistry (IWC, TUM) using atomic emission spectrometry (ELEX 6361, Eppendorf) with an analytical uncertainty of less than ± 5 %.

For elemental concentration analyses of the rock samples, the material was milled and a portion of 1.5 g was digested in aqua regia regarding DIN EN 13657 [69]. The elemental concentrations of rock samples were determined using an ICP-OES (calcium, magnesium, potassium, sodium and silicon) or ICP-MS (boron, rubidium, lithium and strontium) according to DIN EN ISO 11885 and 17294-2 [70,71] in the laboratory of Görtler Analytical Services GmbH.

3.3.2. Stable water isotopes of water samples

The determination of stable water isotope ratios of hydrogen ($^2H/^1H$) and oxygen ($^{18}O/^{16}O$) of water samples was performed with a laser-based analyser (Los Gatos IWA-45EP) at the Chair of Hydrogeology, TUM with an analytical precision of ±1 ‰ for δ^2H and ±0.1 ‰ for $\delta^{18}O$. The stable water isotope ratios were expressed in the δ-notation (δ^2H and $\delta^{18}O$) with respect to the IAEA-standard reference materials VSMOW (Vienna-Standard Mean Ocean Water).

3.3.3. Strontium isotope analyses

To determine the influence and interaction processes of the groundwater with the individual minerals that compose the aquifer rocks (calcite, dolomite and silicate residuals), the strontium isotopes were measured in different leaching fractions of the rock samples.

For Sr-isotope analyses of rock and vein samples, 10 to 30 g of the milled material was transferred in pre-cleaned 250 ml PP bottles for stepwise leaching experiments [72]. The easily soluble fraction of calcite (LF 1) was leached with 0.1 M HCl. This fraction is assumed to be most affected during water-rock interaction processes under reservoir conditions.

After removing the first leaching fraction LF 1, the residual calcite of all samples of SS and MS was leached with 0.5 M HCl (LF 2). Subsequently, the remaining sample was dissolved after separation of the LF 2 fraction by addition of 2.0 M HCl at 80 °C to receive

Preprints (www.preprints.org) | NOT PEER-REVIEWED | Posted: 8 October 2022 doi:10.20944/preprints202210.0090.v1

the dolomite (LF 3) fraction. After the removal of all carbonate fractions, the silicate residuals were completely digested in HF/HNO_3 (3:1) in a PFA container at 140 °C for analysing the residual fraction. In addition to the stepwise leaching, $^{87}Sr/^{86}Sr$ ratios of the bulk rock sample were also determined using an additional milled sample aliquot. Bulk rock samples for $^{87}Sr/^{86}Sr$ analyses were digested in PFA vials using an HF/HNO_3 mixture (3:1) at 140 °C.

For selected samples of GEN, the leaching protocol was modified. After removing the first leaching fraction LF 1 of the sample, the remaining aliquot was dissolved directly in 2.0 M HCl at 80 °C to obtain the heavily soluble calcite and dolomite fraction of these samples (LF 2+3).

The $^{87}Sr/^{86}Sr$ ratios of water and rock samples were measured by thermal ionization mass spectrometry (TIMS; VG Sector 54) in the laboratory of IsoAnalysis UG (Berlin). Prior to TIMS analyses all samples were subjected to ion-chromatographic strontium/matrix separation. An aliquot of each water and rock sample contained about 2 µg Sr and was firstly evaporated, then dissolved in 3.0 M HNO_3, again evaporated and finally dissolved in 0.35 mL 3.0 M HNO_3. Strontium/matrix separation was performed using the Sr-Spec resin from Eichrom® on mini-columns (volume 0.7 mL), following a method by [73]. Strontium isotope analyses were performed with 200 ng Sr by dynamic multi-collection. The TIMS raw data were evaluated using the internationally accepted convention method [74]. Interfering rubidium was substracted using the measured Rb^+ intensity on mass 85. Mass fractionation was corrected using an $^{86}Sr/^{88}Sr$ ratio of 0.1194 and the $^{87}Sr/^{86}Sr$ data were finally normalized to an $^{87}Sr/^{86}Sr$ ratio of 0.71025 for NIST SRM 987.

For $^{87}Sr/^{86}Sr$ ratios, the accuracy and reproducibility were controlled by analysing the seawater reference material NASS-6. While the 2SE in-run-precision of $^{87}Sr/^{86}Sr$ measurement was typically below 0.000015, a small number of rock and water samples instead achieved higher in-run precisions. The measurement results for the NASS-6 reference material show an $^{87}Sr/^{86}Sr$ ratio of 0.709178 (±0.000033 2SD, N=14), which is in excellent agreement with the reference value for open seawater of 0.70976 (GeoRem database Nass-6 and IAPSO). The expanded measurement uncertainty (U k=2) for $^{87}Sr/^{86}Sr$ ratios has been calculated at 0.000050.

The determination of the strontium isotopes of the samples within the Interreg IIIa [33] project from the Wilsingen (W) borehole was performed on a leaching fraction dissolved with 0.05 M HCl only. An aliquot of water contained about 1 µg of strontium and was subsequently evaporated under an IR lamp, dissolved in 1 ml of 12 M HCl, and evaporated again. Then, it was dissolved in 0.5 ml of 5 N HNO_3 for ion exchange separation of Sr using Eichrom® Sr spec resin. Subsequently, the Sr-isotope analysis was performed using TIMS Triton (Thermo Finnigan).

3.3.4. Boron isotope analyses

The measurements of rock and water samples were performed in the laboratories of IsoAnalysis UG (Berlin). Boron isotope ratios of rock samples were determined on individual sample aliquots of about 100 mg milled rock material after dissolving the carbonate fraction in one step with 2 M HCl. Water samples were measured after boron/matrix separation (micro-sublimation) by TIMS (VG Sector 54) and rock samples by MC-ICP-MS (Thermo Fisher Scientific, Neptune). TIMS and MC-ICP-MS measurements were performed using the $Cs_2BO_2^+$ [75] and B^+ standard-sample bracketing technique [73], respectively. Prior to the isotope ratio measurements, the micro-sublimation technique [76] was used to separate boron from natural sample matrices. The micro-sublimation was carried out in conical PFA conical vials at 110 °C for 16 hours.

For rock samples, quality control was performed with the carbonate reference material JCp-1 (coral). The measurement results for the JCp-1 display an $\delta^{11}B$ value of +23.5 ‰, which is about 0.8 ‰ higher than the reference value of +24.3 ‰ (GeoRem database). Due to a relatively low boron concentration of the analysed rock samples, the expanded measurement uncertainty for $\delta^{11}B$ of rock samples was estimated to about ±4 ‰.

Preprints (www.preprints.org) | NOT PEER-REVIEWED | Posted: 8 October 2022 doi:10.20944/preprints202210.0090.v1

For water samples, accuracy and reproducibility were controlled by analysing the certified isotope reference material NIST SRM 951a and the groundwater reference material IAEA B3. The measurement results for the IAEA B3 standard displays an $\delta^{11}B$ value of -21.2 ‰, which is in excellent agreement with the reference value of -21.3 ‰ [77]. Based on the reproducibility of the NIST SRM 951a, the reference material measurements and the accuracy of the quality control sample IAEA B3, the expanded measurement uncertainty for $\delta^{11}B$ of water samples was estimated to ±0.8 ‰.

Table 1. Investigated rock sample description with designated number displayed on Figure 1.

Sample	Borehole	Chronostratigraphic levels	Characterisation	Depth below surface / Top Malm [m TVD]
W1	Wilsingen (W)	Upper Kimm.	Limestone	85
W2		Upper Kimm.	Limestone	110
W3		Lower Kimm.	Lime marl	145
W4		Lower Kimm.	Limestone	200
SS	SS	Tithonian	Ooid grainstone	4,300 / 158.1
MS1	Moosburg (MS)	Tithonian	Limestone	1,127 / 12
MS2		Tithonian	Dolostone	1,254 / 139
MS3		Kimmeridgian	Dolostone	1,424 / 309
MS4		Oxfordian	Lime marl	1,540 / 425
GS1	Geretsried GEN-1ST-A1 (GEN)	Upper Kimm.	Micrite	4,595 / 185.4
GS2		Upper Kimm.	Micrite	4,595.1 / 185.5
GS3		Upper Kimm.	Micrite	4,600 / 190.4
GS4		Upper Kimm.	Micrite	4,600,5 / 190.9
GS5		Upper Kimm.	Micrite	4,649,8 / 240.2
GS6		Upper Kimm.	Micrite	4,655,5 / 245.9
GS7		Upper Kimm.	Micrite	4,656 / 246.4
GS8		Upper Kimm.	Micrite / Wackestone	4,706.2 / 296.6
GS9		Upper Kimm.	Micrite / Wackestone / Dolostone	4,710.3 / 300.7
GS10		Upper Kimm.	Micrite / Wackestone /Dolostone	4,710.9 / 301.3
GV1		Upper Kimm.	Vein Calcite	4,634.5 / 224.9
GV2		Upper Kimm.	Vein Calcite	4,709 / 299.4
GV3		Upper Kimm.	Vein Calcite	4,709.5 / 299.9

3.3.4. Stable isotope analyses of vein calcite samples

For the analyses of the stable isotopes $^{13}C/^{12}C$ and $^{18}O/^{16}O$ of the selected vein samples, 200 mg of rock material was transferred to a 20 ml headspace vial. A test tube was filled with 1.0 g of phosphoric acid (100 %) and transferred into the head space vial. The vial was flushed by helium and afterwards capped with a crimper. After heating the vial up to 50 °C, the phosphoric acid liquidated, and the vial was stirred until the acid and the vein sample were well mixed. The vial rested 24 h until all carbonate fractions were converted to CO_2, immediately after conversion by an elemental analyser-isotope ratio mass spectrometry (EA-IRMS) consisting of a Thermo Scientific Flash 2000 EA (Thermo Fisher Scientific, Milan, Italy) coupled to a IRMS Delta V plus (Thermo Fisher, Scientific, Bremen,

Preprints (www.preprints.org) | NOT PEER-REVIEWED | Posted: 8 October 2022 doi:10.20944/preprints202210.0090.v1

Germany) by a Conflow IV (Thermo Fisher Scientific, Bremen, Germany). The $^{13}C/^{12}C$ and $^{18}O/^{16}O$ ratios are expressed in the δ-notation with reference to the IAEA international standard V-PDB (Vienna-Pee-Dee-Belemnite) and the measurement error of the double determination was ±0.5 ‰ for $\delta^{13}C$ and ±0.2 ‰ for $\delta^{18}O$.

4. Results and Discussion

4.1. Rock sample measurements

All analytical results from the rock samples are presented in **Table 2**. Figure 2 shows the molar composition and the measured $^{87}Sr/^{86}Sr$ ratios of the Upper Jurassic carbonate rocks from the Wilsingen (W), Moosburg (MS), SS and Geretsried (GS) borehole samples in relation to their relative depth from the top of the Upper Jurassic formation.

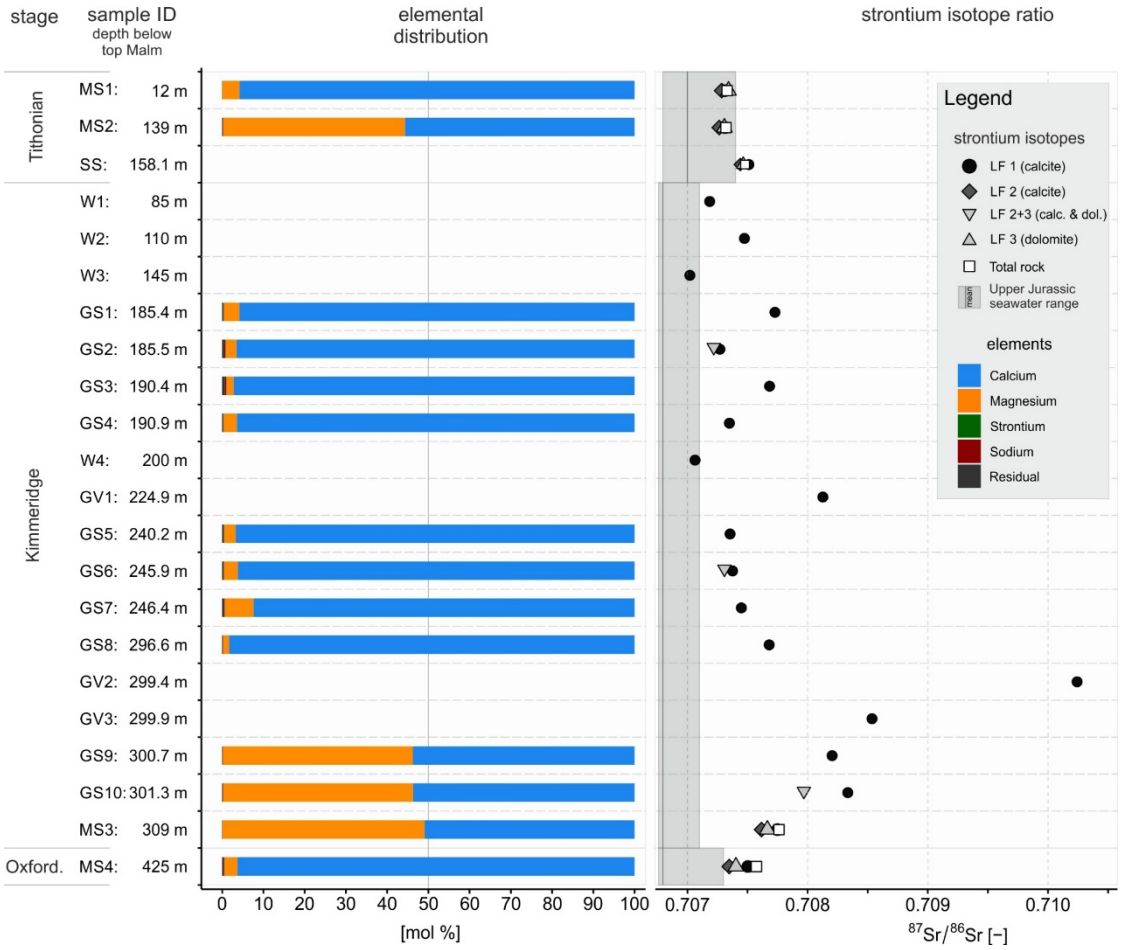

Figure 2. Analysed carbonate samples from Upper Jurassic drill cores displayed in their depth from top of the Upper Jurassic, with the metal composition and the strontium isotope values of the different fractions and Upper Jurassic strontium isotope signature distribution from literature [34,78,79].

4.1.1. Elemental composition and 87Sr/86Sr isotope ratios of Upper Jurassic rocks

In general, the investigated Upper Jurassic rock samples are mostly composed of calcite and dolomite, with calcium as the major metal element (**Figure 2**). Only the four samples MS2, MS3, GS9 and GS10 contain a considerable amount of magnesium with up to 48 Mol-%, implying a higher dolomite abundance. The concentration of the remaining elemental parameters strontium, sodium, potassium, lithium, rubidium, silicon and boron are either neglectable low or below the specific detection limit. These values (**Table 2**) are in accordance to literature data [80].

Preprints (www.preprints.org) | NOT PEER-REVIEWED | Posted: 8 October 2022 doi:10.20944/preprints202210.0090.v1

The $^{87}Sr/^{86}Sr$ signatures of the three leaching fractions (LF 1 to LF 3) from the samples MS1 to MS4 and SS show only minor variations compared to the bulk signature of the total rock for each sample (**Table 2**, **Figure 2**, **Figure 3**).

The first fraction (LF 1, 0.1 M HCl (MS, SS, GS) or 0.05 M HCl (W)), which represents the easily soluble calcites, may be expected to be prone to ongoing water-rock-interaction processes. $^{87}Sr/^{86}Sr$ ratios of the LF 1 fraction of all rock samples (W, SS, MS and GS) comprise a wide range from 0.70702 (W3) to 0.708334 (GS10), which includes all further analysed leached carbonate fractions. Moreover, the $^{87}Sr/^{86}Sr$ ratios of LF 1 of MS and SS indicate only a small deviation of $<1 \times 10^{-4}$ from the bulk rock analysis (Table 2, Figure 2, Figure **3**).

The second fraction (LF 2, 0.5 M HCl) of the samples MS1 to MS4 and SS results from the complete dissolution of calcite after removing the easily soluble LF 1. For the individual rock samples, the LF 2 represents the lowest $^{87}Sr/^{86}Sr$ ratio. Although the values of LF 2 show the lowest deviation from the Phanerozoic seawater curve (**Figure 3**), the differences tend to be considerably higher than the internal variation of the leaching fractions for each sample.

The LF 3 (2.0 M HCl), which represents primarily the dolomites, reveals a slight increase in the $^{87}Sr/^{86}Sr$ ratios compared to LF 2 for each sample of MS1 to MS4 and SS. Except for MS1, all $^{87}Sr/^{86}Sr$ ratios of LF 3 are below the $^{87}Sr/^{86}Sr$ ratio of LF 1 and the bulk rock. These LF 2 and LF 3 fractions are most probably responsible for the lower $^{87}Sr/^{86}Sr$ ratios of the bulk rock samples compared to the LF 1 for MS1, MS2 and SS. In contrast, the $^{87}Sr/^{86}Sr$ ratios of bulk rock of the samples MS3 and MS4 are slightly higher than the leaching fractions, which might be caused due to the influence of silicate residuals in the bulk rock analysis.

The LF 2+3 fractions of GS2, GS6 and GS10 represent both, the residual calcites (LF 2) and the dolomites (LF 3), as these samples were digested only with 2.0 M HCl directly after the LF 1 fraction was separated. The $^{87}Sr/^{86}Sr$ signature of the LF 2+3 fraction of the samples GS2 and GS6 are very similar and only slightly elevated compared to LF 1. In contrast, LF 2+3 of GS10 (0.707969) are considerably higher and more radiogenic than all other samples (LF 2, LF 3 and LF 2+3) of the Kimmeridge. Additionally, LF 1 of GS10 is deviating to an even higher radiogenic value (0.708334).

Residuals were only analysed in the samples MS1, MS2 and SS. The $^{87}Sr/^{86}Sr$ ratios equal 0.708333 for MS1 and 0.724222 and 0.750162 for MS2 and SS, respectively. It is reasonable that the residuals do not have a considerable impact on the $^{87}Sr/^{86}Sr$ signatures of the bulk rock analyses for these rock samples as the content of silicates and other residual elements are negligible in Upper Jurassic carbonates with less than 1 mol-% (**Table 2**, **Figure 2**).

The three samples GV1 to GV3 originate from calcite vein fillings of the Kimmeridgian carbonates of the Geretsried drill core (GEN) at different depths. The $^{87}Sr/^{86}Sr$ ratios range from 0.708127 (GV1) in a depth of 224 meters below the top of Upper Jurassic formation to values of 0.708535 (GV3) and 0.710244 (GV2), respectively. GV2 was located only 0.5 m above the sample GV3 in a depth of around 300 meters below the top of the Upper Jurassic formation. The two $^{87}Sr/^{86}Sr$ values (GV2 and GV3) are significantly different from each other and considerably elevated compared to the analysed LF 1 fraction of the surrounding rock samples at comparable depths (GS8 to GS10) of the sampled profile of GEN (**Figure 2**).

For the vein samples GV1 and GV2, analyses of stable carbon and oxygen isotopes of $CaCO_3$ resulted in similar values for $\delta^{13}C\text{-}CaCO_3$ (-2.9 ‰) and only slightly different signatures for $\delta^{18}O\text{-}CaCO_3$ (-19.5 ‰ at GV1 and -18.5 ‰ at GV2). The stable isotope composition of both vein calcites indicates formation temperatures that are too low for the burial depth of the Upper Jurassic. The difference in the $^{87}Sr/^{86}Sr$ ratios of both samples GV1 and GV2 along with the comparable and low values for $\delta^{13}C\text{-}CaCO_3$ and $\delta^{18}O\text{-}CaCO_3$ indicate

 doi:10.20944/preprints202210.0090.v1

that various low tempered fluids with different carbon isotope composition and radiogenic strontium have precipitated in the veins of the Upper Jurassic rocks, which is also in accordance to Mraz [41].

4.1.2. Processes on strontium isotope systematics of rocks

The paleo $^{87}Sr/^{86}Sr$ seawater curve represents the typical strontium isotope ratios of seawater during the Phanerozoic and was reconstructed using common signatures of fossils and marine rocks [31]. For the carbonates of the Upper Jurassic, $^{87}Sr/^{86}Sr$ ratios between 0.70676 to 0.70742 were determined by various authors [29,34,78,79]. In this study, the results of the analysed Upper Jurassic rock samples, show overall elevated values in comparison to the signatures of the Upper Jurassic seawater curve (**Figure 2**, **Figure 3**). This indicates a considerable radiogenic influence on the Upper Jurassic carbonates in the SGMB.

Because the strontium isotope signatures of all leaching fractions as well as the bulk rock samples are significantly above the Upper Jurassic seawater curve, it is not plausible that post-depositional fluid events homogeneously altered the entire Upper Jurassic carbonates. Intensive strontium exchange of the carbonates with the residuals can also be neglected due to the strontium mass balance with minor portions of residuals (< 1 mol %) within the rock samples (**Figure 2**). Therefore, the elevated signatures may instead result from a pre- or syn-depositional radiogenic input by exogenic processes. The radiogenic strontium isotope input may be associated with the crystalline Bohemian massif in the east of the Upper Jurassic offshore zone. Weathering products of crystalline rocks might have been transported by rivers into the marine depositional area [81]. Based on this, plausible differences occur in the $^{87}Sr/^{86}Sr$ signatures between the rock samples of different stratigraphic levels and areas within the SGMB, e.g. the Thitonian samples of MS and SS, but also within the Kimmeridge succession as expressed in the LF 1 data set of GS (Table 1, Figure 3).

Except for GS10 (LF 1 and LF 2+3), the carbonate fractions (LF 1 (calcite) to LF 3 (dolomite)) within each rock sample of MS and SS show only minor internal differences. Therefore, secondary processes or fluid events for different carbonate fractions cannot be identified in general. Contributing to the findings of marine induced early diagenetic dolomitisation by other authors [45,82,83], this highlights that not only calcite but also dolomite formation had been in equilibrium with the regional marine environment.

The comparison of the total range of $^{87}Sr/^{86}Sr$ values in the LF 1 of GS to the vein calcites (GV 1 to GV 3) suggests that after deposition, secondary fluids with distinct radiogenic $^{87}Sr/^{86}Sr$ signatures have circulated through the Upper Jurassic rock section. As the dolomite dominated sample GS10 shows the highest $^{87}Sr/^{86}Sr$ signature in LF 1 and the total carbonate fraction LF 2+3 reveals a lower deviation to the seawater curve than LF 1, these fluids might have preferentially affected LF 1 in the Upper Jurassic carbonates. This can be attributed to the influence of the adjacent vein fillings (GV2 and GV3) on LF 1, which are most likely originating from secondary and exogenous low tempered fluids.

The comparison of the MS to GS drill core samples highlights the variability of $^{87}Sr/^{86}Sr$ signatures of the LF 1 fraction due to secondary processes in contrast to the $^{87}Sr/^{86}Sr$ signatures of the total carbonate fractions of LF 2 and LF 3 for the central SGMB.

The $^{87}Sr/^{86}Sr$ ratios of LF 1 of the most western samples (well W, **Figure 1**) are generally very low and close to the typical values of the Upper Jurassic seawater curve (Figure 3), which is in accordance to its distal depositional area and the lower influence of the Bohemian Massif. Thereby, sample W2 represents an exception and instead originates from an active karst zone. Here, the relatively high $^{87}Sr/^{86}Sr$ ratio (0.70747) is most probably imprinted by the interaction with locally circulating younger groundwater [33] that is characterised by a considerably higher $^{87}Sr/^{86}Sr$ signature of 0.70844 (sample 38, **Table 3**).

In summary, circulating fluids at karstification zones and/or fractures may preferentially have a considerable influence on the LF 1 fraction of carbonate rocks via isotope exchange reactions. The carbonate fractions LF 2 and LF 3 do not show obvious influences

Preprints (www.preprints.org) | NOT PEER-REVIEWED | Posted: 8 October 2022 doi:10.20944/preprints202210.0090.v1

of secondary post-depositional processes to the same extend. Thus, both display rather invariable $^{87}Sr/^{86}Sr$ signatures and likely have $^{87}Sr/^{86}Sr$ signatures close to the initial signature that was generated during carbonate formation.

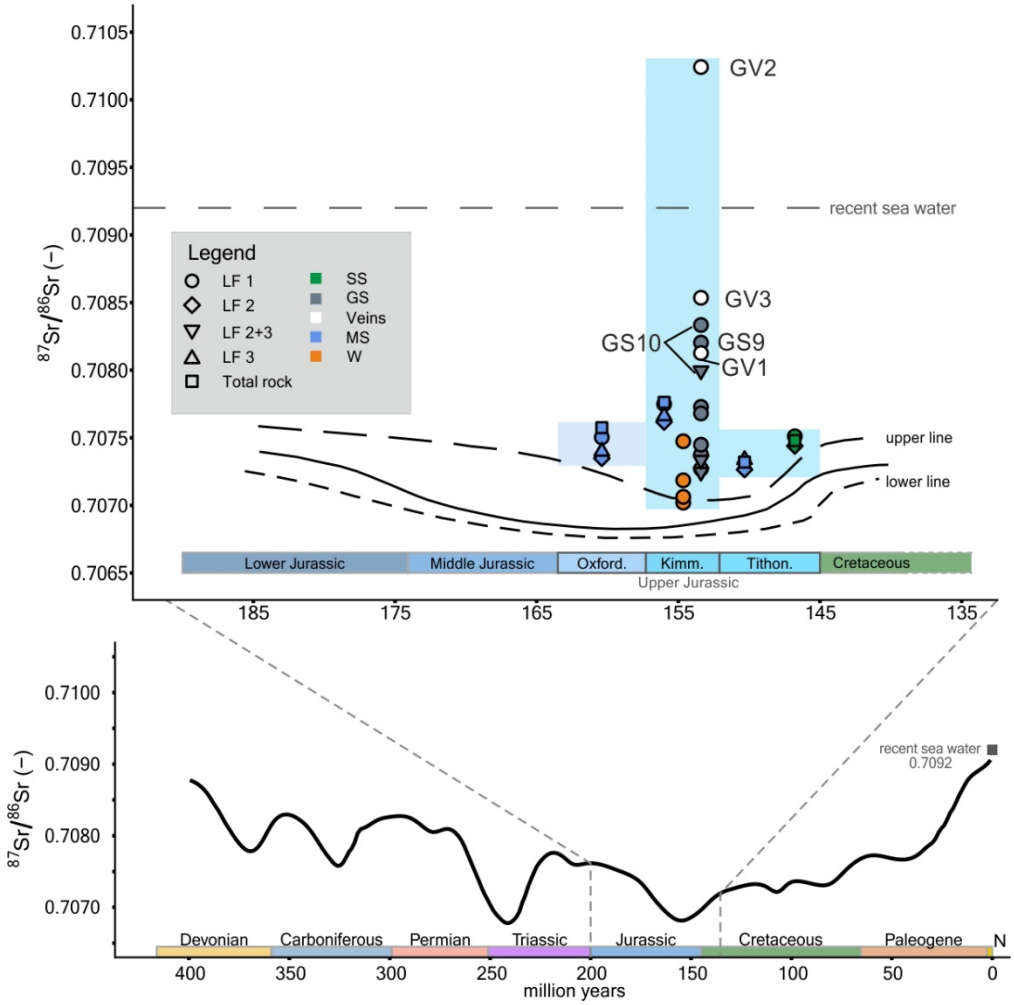

Figure 3. Comparison of $^{87}Sr/^{86}Sr$ signatures of the investigated Upper Jurassic carbonates with the Phanerozoic seawater curve according to the literature [34,78,79].

4.1.3. Boron isotope composition of Upper Jurassic rocks

For the Upper Jurassic carbonate rocks of the SGMB there are no boron isotope data available so far. Due to elevated boron contents in the hydrochemical composition of the thermal waters of the central SGMB, three samples (SS, MS1, and MS4) were selected regarding the boron isotope signature of the total carbonate fraction. The examined aliquot corresponds to LF 1 to 3.

The boron content of the rock samples range between 0.4 and 3.8 mg/kg (**Table 2**) and are very low compared to literature data of marine carbonate rocks, which vary between 1 and 100 mg/kg [39]. The $\delta^{11}B$ values of these total carbonate samples are +15.3 ‰ (MS1), +9.6 ‰ (MS4) and -1.6 ‰ (SS) with an uncertainty of ±4 ‰.

While modern open seawater typically has a $\delta^{11}B$ value of +40 ‰ [39],Upper Jurassic seawater was reconstructed to $\delta^{11}B$ values between +39.0 and +41.5 ‰ [37,39,68]. By using fractionation factors for carbonate precipitation from seawater between -16.5 ‰ [84] and -27.2±0.6 ‰ ([85]), despite potential kinetic effects, the lower $\delta^{11}B$ limit for Upper Jurassic carbonates precipitated directly from seawater can be estimated to values ranging from +13 ‰ to +25 ‰. In comparison, the three Upper Jurassic samples, especially SS (-1.6 ‰) and MS4 (+9.6 ‰), show considerably lower and depleted $\delta^{11}B$ values than the estimated

Preprints (www.preprints.org) | NOT PEER-REVIEWED | Posted: 8 October 2022 doi:10.20944/preprints202210.0090.v1

values for Upper Jurassic carbonates (**Figure 4**). Therefore, it may be assumed that the analysed Upper Jurassic carbonates of MS1, MS4 and SS were affected either by secondary processes during diagenesis (e.g. water-rock interactions with $\delta^{11}B$ depleted fluids) or pre- to syn-depositional input of terrestrial boron with lower $\delta^{11}B$ values (granites show values below 0 ‰ [86]).

The strontium isotopic signatures also show a similar deviation from seawater, which can be attributed to a slight radiogenic or terrestrial input, as discussed above. It seems reasonable, that this input also shifts the boron isotope signatures. If so, the isotopic characteristics of both elements would suggest terrestrial input from weathering of crystalline rock into the marine depositional area of the Upper Jurassic seawater (**Figure 4**).

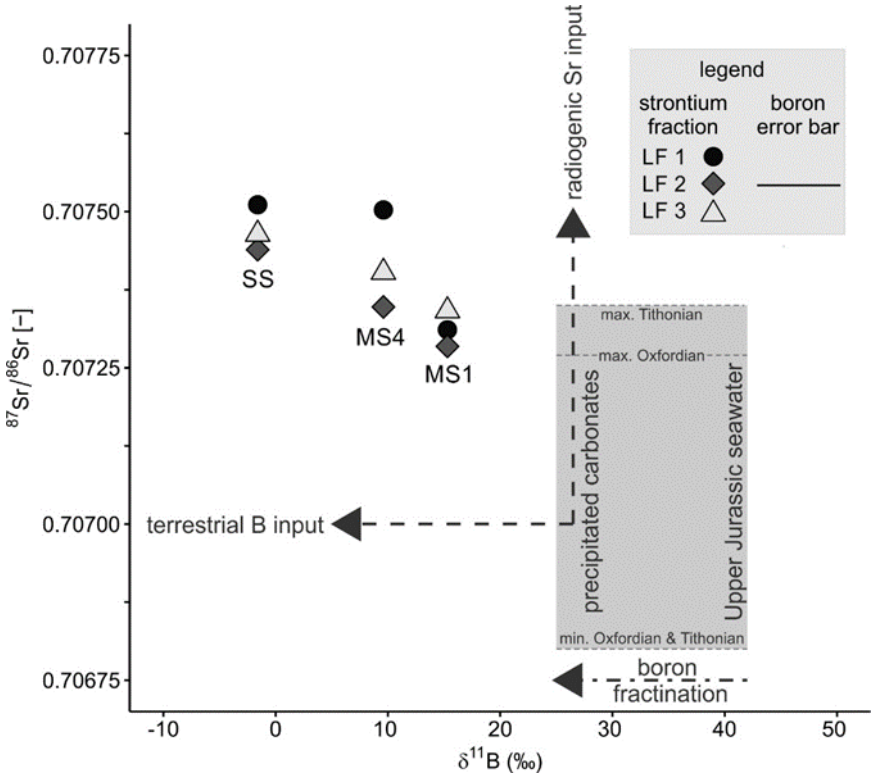

Figure 4. Plot of the strontium and the boron isotope signatures with the carbonate samples from the Upper Jurassic sections of the SS and MS drill cores.

Preprints (www.preprints.org) | NOT PEER-REVIEWED | Posted: 8 October 2022 doi:10.20944/preprints202210.0090.v1

Table 2. Results from rock samples of strontium, boron, carbon and oxygen isotope analyses and metal measurements. Boron concentrations with ++ were measured separately during the determination of the boron isotopes.

ID	$^{87}Sr/^{86}Sr$ ratio [-]					$\delta^{11}B$	$\delta^{13}C$	$\delta^{18}O$	Ca^{2+}	Mg^{2+}	Sr^{2+}	K^{+}	Na^{+}	Rb^{+}	Si	B
	LF1 (calcite)	LF2 (calcite)	LF3/LF2 +3 (dol.)	Residual	Bulk rock	[‰]	[‰]	[‰]	mg/kg	mg/kg	mg/kg	mg/kg	mg/kg	mg/kg	mg/kg	mg/kg
W1	0.707185															
W2	0.707474															
W3	0.707020															
W4	0.707063															
SS	0.707511	0.707439	0.707464	0.750162	0.707479	-1.6										0.4++
MS1	0.707311	0.707284	0.707341	0.708333	0.707330	15.3			3.8×10^5	1.0×10^4	120	<50	81	<5	<10	0.4++
MS2	0.707312	0.707265	0.707307	0.724222	0.707320				2.5×10^5	1.2×10^5	67	180	280	<5	240	12
MS3	0.707749	0.707616	0.707665		0.707762				2.4×10^5	1.4×10^5	50	55	85	<5	99	<3
MS4	0.707503	0.707348	0.707403		0.707575	9.6			3.3×10^5	6.6×10^3	270	490	470	<5	220	3.8++
GS1	0.707728								4.0×10^5	9.5×10^3	750	560	250	<5	260	<3
GS2	0.707270		0.707219						3.2×10^5	5.2×10^3	270	1500	550	<5	120	4
GS3	0.707683								3.3×10^5	3.7×10^3	420	1700	660	7.5	160	4.8
GS4	0.707349								3.9×10^5	7.9×10^3	730	300	230	<5	210	<3
GS5	0.707354								4.1×10^5	7.2×10^3	830	750	260	<5	290	4.1
GS6	0.707375		0.707307						4.1×10^5	8.7×10^3	350	760	260	<5	300	3.8
GS7	0.707449								3.7×10^5	1.7×10^4	330	1200	380	<5	270	5.5
GS8	0.707680								4.2×10^5	3.9×10^3	170	120	210	<5	190	<3
GS9	0.708204								2.5×10^5	1.3×10^5	98	140	220	<5	100	<3
GS10	0.708334		0.707969						2.5×10^5	1.3×10^5	87	160	310	<5	220	<3
GV1	0.708126						-2.9	-19.5								
GV2	0.710242						-2.9	-18.5								
GV3	0.708535															

Preprints (www.preprints.org) | NOT PEER-REVIEWED | Posted: 8 October 2022 doi:10.20944/preprints202210.0090.v1

Table 3. Results of hydrochemical analysis, water and boron isotope signature and strontium isotope ratios. Missing Data (*) are completed with hydrochemical analyses from reports. Sample 14 contains 4158 mg/l acetate. Samples with ⁻ originate from surface water/springs.

No.	pH	Ca^{2+}	Mg^{2+}	Na^{+}	K^{+}	Sr^{2+}	HCO_3^{-}	Cl^{-}	SO_4^{2-}	F^{-}	B	TDS	Mg/Ca	Type	$\delta^{18}O$	δD	$^{87}Sr/^{86}Sr$	$\delta^{11}B$
	[-]	mg/l	mg/l	mg/l	mg/l	mg/l	mg/l	mg/l	mg/l	mg/l	mg/l	g/l	molar		‰	‰	[-]	‰
Tertiary: Upper Freshwater Molasse (OSM)																		
1	7.1	91.1	28.7	4.4	1.2	0.82	390.2	1.4	38.6	0.1		0.56	0.52	Ca-Mg-HCO_3	-10.7	-76.1	0.70938	
2	7.0	113.0	38.2	5.5	1.1	0.29	418.3	15.8	51.0	0.1		0.64	0.56	Ca-Mg-HCO_3	-10.1	-70.7	0.70968	
3	7.1	125.0	31.7	4.8	1.1	0.53	421.3	16.3	72.7	0.1		0.67	0.42	Ca-Mg-HCO_3	-10.2	-73.6	0.70906	
4	7.1	129.0	33.2	4.6	0.8	0.29	485.4	7.1	49.5	0.1		0.71	0.42	Ca-Mg-HCO_3	-10.2	-71.7	0.70949	
5	7.1	102.0	24.7	4.1	1.2	0.59	381.7	7.1	38.8	0.1		0.56	0.40	Ca-Mg-HCO_3	-10.1	-73.6	0.70929	
6	7.4	70.5	31.4	9.3	1.0	0.29	347.8	1.3	7.8			0.47	0.73	Ca-Mg-HCO_3	-10.2	-73.4	0.71100	
7	6.9	139.0	17.8	3.2	1.7	0.23	435.4	10.1	14.2			0.62	0.21	Ca-HCO_3	-9.3	-65.5	0.70853	
8	7.2	80.2	33.3	4.6	1.0	1.40	371.3	1.7	40.8			0.53	0.68	Ca-Mg-HCO_3	-10.7	-75.8	0.70963	
9	7.6	60.4	10.6	6.3	1.7	0.43	193.3	8.4	33.5			0.31	0.29	Ca-Mg-HCO_3	-11.3	-81.3	0.70850	
10	7.0	128.0	34.7	12.0	6.8	0.89	487.8	24.6	39.7	0.1		0.73	0.45	Ca-Mg-HCO_3	-9.9	-70.6	0.70961	
Tertiary: Upper Marine Molasse (OMM)																		
11	8.0	20.5	5.6	375.7	18.7	0.38	695.0	181.2	<3.9	12.5	2.42	1.31	0.45	Na-HCO_3-Cl	-10.2	-78.3	0.70993	
12*	8.2	12.8	3.4	862.4		1.04	585.8	753.5	139.0		3.2	2.36	0.44	Na-Cl-HCO_3	-9.3	-68.1	0.70881	
Tertiary: Lower Freshwater Molasse (USM)																		
13*	8.4	4.2	1.1	715.0	5.2	0.17	1281.0	90.8	8.9	7.0	6.3	2.11	0.42	Na-HCO_3	-10.5	-74.7	0.70939	
Tertiary: Lower Marine Molasse (UMM)																		
14*	7.3	255.7	34.0	7075.6	69.5	25.3	365.1	8590.9	7.6	1.5	3.63	20.58	0.22	Na-Cl-HCO_3	5.2	-14.6	0.70828	
Cretaceous aquifer																		
15	7.4	40.5	18.1	104.9	11.0	0.89	402.7	63.9		2.3	0.76	0.64	0.73	Na-Ca-HCO_3-Cl	-11.6	-84.9	0.70932	
Upper Jurassic reservoir: Ca-I																		
16	7.4	89.0	22.6	7.1	0.6	0.07	274.6	63.1		2.9		0.46	0.42	Ca-Mg-HCO_3-Cl	-9.9	-69.8	0.70837	
17	7.5	80.9	22.2	5.7	0.9	0.17	463.7	4.3	7.9		1.26	0.59	0.45	Ca-Mg-HCO_3	-9.6	-69.3	0.70863	
18	7.6	51.6	31.1	20.8	3.4	0.74	349.8	2.8	11.2	1.3		0.47	0.99	Ca-Mg-HCO_3	-9.9	-69.0	0.70762	
19	7.6	75.4	7.5	18.1	2.6	0.18	197.1	30.0	41.2	0.2		0.37	0.16	Ca-HCO_3	-9.7		0.70872	
20	7.2	66.1	26.2	10.8	2.3	0.57	335.6	4.3	12.5	0.3		0.46	0.65	Ca-Mg-HCO_3	-10.0	-69.8	0.70793	
21	7.7	36.5	48.0	18.6	5.2	2.90	294.9	3.3	78.3	2.4		0.49	2.17	Mg-Ca-HCO_3-SO_4	-10.4	-74.7	0.70741	
22	7.2	123.0	3.0	10.9	0.9	0.05	343.9	25.8	8.8			0.52	0.04	Ca-HCO3	-10.4	-73.4	0.70822	
23	7.2	118.0	3.0	10.6	0.9	0.05	337.2	25.6	8.7			0.50	0.04	Ca-HCO3	-10.4	-73.6	0.70822	
24	7.8	71.5	26.4	45.9	3.9	1.70	391.2	6.2	60.8	1.2		0.61	0.61	Ca-Mg-HCO3	-10.1	-72.4	0.70763	
25	7.9	43.2	22.9	13.9	4.0	0.68	268.3	2.7	10.3	0.3		0.37	0.87	Ca-Mg-HCO3	-9.8	-68.6	0.70816	
26	7.3	112.0	2.1	1.5	0.3	0.05	326.2	3.1	9.2			0.45	0.03	Ca-HCO3	-10.2	-69.3	0.70825	
27	7.2	120.0	2.3	4.1	0.6	0.05	345.1	9.7	12.9			0.49	0.03	Ca-HCO3	-10.2	-71.9	0.70827	
28	7.5	105.0	3.1	0.7	0.7	0.07	324.4	1.5	12.5			0.45	0.05	Ca-HCO3	-9.9	-69.0	0.70843	
29	7.2	115.0	2.9	8.1	1.4	0.05	333.5	14.7	8.3			0.48	0.04	Ca-HCO3	-10.3	-71.3	0.70807	
30	7.0	65.3	18.6	24.7	3.1	0.73	329.5	7.3	10.6	1.3		0.46	0.47	Ca-Mg-HCO3	-10.0	-69.6	0.70838	
31	7.3	140.0	7.8	10.1	1.9	0.44	442.0	16.6	9.1	0.2		0.63	0.09	Ca-HCO3	-9.9	-70.8	0.70845	
32	7.2	122.0	2.2	7.7	0.7	0.19	335.4	21.7	10.2			0.50	0.03	Ca-HCO3	-10.1	-72.3	0.70866	
33	7.2	125.0	2.7	4.7	0.8	0.04	339.6	15.3	14.9			0.50	0.04	Ca-HCO3	-10.3	-73.2	0.70854	
34	7.0	85.7	20.7	4.8	1.7	0.36	343.9	7.1	10.2	0.2		0.47	0.40	Ca-Mg-HCO3	-10.5	-74.4	0.70818	
35	7.3	52.1	19.7	33.5	3.9	0.91	305.0	6.6	23.0	1.8		0.45	0.62	Ca-Mg-HCO3	-10.6	-72.9	0.70797	
36	7.2	106.0	9.3	4.7	1.0	0.07	320.1	15.6	9.1			0.47	0.14	Ca-HCO3	-10.0	-71.0	0.70841	
37	7.4	96.1	2.2	9.6	1.6	0.16	252.4	21.1	14.5	0.2		0.40	0.04	Ca-HCO3	-9.5	-66.6	0.70817	

 doi:10.20944/preprints202210.0090.v1

No.	pH	Ca^{2+}	Mg^{2+}	Na^{+}	K^{+}	Sr^{2+}	HCO_3^{-}	Cl^{-}	SO_4^{2-}	F^{-}	B	TDS	Mg/Ca	Type	$\delta^{18}O$	δD	$^{87}Sr/^{86}Sr$	$\delta^{11}B$
	[-]	mg/l	mg/l	mg/l	mg/l	mg/l	mg/l	mg/l	mg/l	mg/l	mg/l	g/l	molar		‰	‰	[-]	‰
38	7.4	104.0	12.6	7.1	0.8	0.10	350.0	3.6	33.7	0.1		0.51	0.20	Ca-HCO3	-10.2	-70.7	0.70844	
39-	7.3	125.0	3.4	12.4	0.9	0.04	366.1	17.5	7.8			0.53	0.05	Ca-HCO3	-9.8	-68.8	0.70864	
40-	7.3	91.9	28.1	10.0	1.2	0.12	366.1	25.4	32.0			0.55	0.50	Ca-Mg-HCO3	-9.7	-68.5	0.70945	
41-	7.4	66.2	8.6	16.8	2.9	0.10	162.0	28.9	47.7			0.33	0.21	Ca-HCO3	-9.89	-69.3	0.70841	
Upper Jurassic reservoir: Ca-II																		
42	7.3	68.5	20.1	7.5	0.9	0.26	311.2	1.2	8.5			0.42	0.48	Ca-Mg-HCO3	-9.8	-70.9	0.70952	
43	7.2	101.7	22.5	8.4	1.6	0.32	408.8	8.4	11.0			0.56	0.36	Ca-Mg-HCO3	-9.2	-67.4	0.71002	
44	7.2	95.7	24.2	8.1	1.6	0.39	439.3	3.7	9.7			0.58	0.42	Ca-Mg-HCO3	-9.5	-68.2	0.71001	
45	7.3	89.1	33.3	8.3	1.4	0.26	372.2	16.3	19.4			0.54	0.62	Ca-Mg-HCO3	-9.4	-68.5	0.70950	
46	7.5	88.8	34.3	8.9	0.9	0.26	463.7	1.5	22.2			0.62	0.64	Ca-Mg-HCO3	-10.0	-72.1	0.71004	
47	7.4	79.2	31.2	13.1	1.3	0.36	387.5	1.7	19.6			0.53	0.65	Ca-Mg-HCO3	-10.0	-73.4	0.71017	
48	7.7	39.8	13.3	40.0	3.5	0.43	244.1	1.6	15.7	0.5		0.36	0.55	Ca-Na-Mg-HCO3	-12.5	-89.4	0.70918	
49	7.1	134.0	2.5	7.8	1.4	0.08	348.0	19.3	21.9	0.2		0.54	0.03	Ca-HCO3	-9.7	-70.0	0.70912	
50	7.2	130.0	1.1	1.6	0.5	0.04	350.7	7.2	13.1			0.50	0.01	Ca-HCO3	-9.8	-68.4	0.70905	
Upper Jurassic reservoir: Na-Ia																		
51	7.2	33.7	10.7	120.0	14.2	0.57	326.4	72.0	7.8	6.6	2.2	0.59	0.52	Na-Ca-HCO_3-Cl	-11.8	-86.6	0.70926	10.0
52	6.7	24.8	3.7	121.6	15.9	0.65	280.7	77.1	4.3	4.6	2.22	0.53	0.25	Na-HCO_3-Cl	-11.9	-86.6	0.70925	9.4
53	6.8	35.3	10.2	120.0	12.8	0.61	332.5	72.6	6.4	2.8		0.59	0.48	Na-Ca-HCO_3-Cl	-11.9	-86.8	0.70925	
54	6.9	30.4	7.5	122.3	14.7	0.57	302.0	82.5	1.4	2.2		0.56	0.40	Na-HCO_3-Cl	-11.9	-86.3	0.70924	
55	7.0	31.9	8.9	123.8	7.3	0.65	344.7	70.4	2.9	1.8		0.59	0.46	Na-Ca-HCO_3-Cl	-11.6	-85.4	0.70923	
56	7.1	35.1	10.4	122.0	13.8	0.56	323.4	69.8		2.7		0.58	0.49	Na-Ca-HCO_3-Cl	-11.7	-85.9	0.70922	
57	7.1	27.1	7.2	122.5	14.8	0.65	329.5	69.5		1.9		0.57	0.44	Na-HCO_3-Cl	-11.7	-86.2	0.70922	
58	6.9	28.6	8.8	120.9	14.3	0.57	305.1	69.9		3.3		0.55	0.51	Na-HCO_3-Cl	-11.5	-86.2	0.70922	
59	7.1	31.8	9.4	112.0	15.2	0.57	329.5	70.0	1.6	2.4		0.57	0.49	Na-Ca-HCO_3-Cl	-11.7	-86.3	0.70921	
60	6.3	16.6	1.8	134.7	22.9	0.50	250.2	82.2	15.8	5.1		0.53	0.18	Na-HCO_3-Cl	-11.4	-85.1	0.70920	
61	6.4	9.4	1.1	129.2	15.5	0.15	216.6	74.5	5.1			0.45	0.19	Na-Ca-Cl-HCO_3	-11.5	-85.7	0.70909	
62	6.5	3.5	1.6	130.1	17.2	0.16	214.2	74.0	4.1	3.0		0.45	0.74	Na-HCO_3-Cl	-11.6	-86.0	0.70913	
63	6.9	38.5	10.8	129.8	14.6	0.71	354.0	75.6	13.5	5.1	0.68	0.64	0.46	Na-Ca-HCO_3-Cl	-11.7	-86.4	0.70907	9.6
64	6.5	16.9	1.7	121.6	19.8	0.75	256.3	69.1	4.8	2.0		0.49	0.16	Na-HCO_3-Cl	-11.6	-86.5	0.70905	
65	6.4	18.5	2.1	143.5	20.6	0.55	274.6	95.8	13.8	7.9		0.58	0.19	Na-HCO_3-Cl	-11.0	-84.8	0.70902	
66	6.7	23.4	3.1	131.0	21.2	0.59	274.6	81.7	8.2	4.2		0.55	0.22	Na-HCO_3-Cl	-11.8	-86.3	0.70901	
67	6.4	44.0	4.8	194.5	34.0	1.09	305.1	160.0	21.7	2.9		0.77	0.18	Na-HCO_3-Cl	-11.0	-84.2	0.70899	
68	6.5	27.0	3.8	129.1	18.9	0.99	288.3	79.0	12.5	2.7		0.56	0.23	Na-HCO_3-Cl	-11.6	-85.8	0.70881	
69	6.3	42.9	5.3	194.0	34.4	1.40	360.0	155.5	26.3	7.7	3.3	0.83	0.20	Na-HCO_3-Cl	-10.7	-83.9	0.70862	8.6
Upper Jurassic reservoir: Na-Ib																		
70	7.4	20.0	8.6	92.0	7.4	0.48	302.0	32.3	8.9	0.7		0.47	0.71	Na-HCO_3	-11.8	-84.7	0.70812	
71	7.7	23.0	10.0	71.0	5.2	0.45	275.2	27.0	23.7	2.5		0.44	0.72	Na-Ca-HCO_3	-12.6	-90.4	0.70810	
72	7.8	10.5	3.4	205.0	4.3	0.44	376.8	75.6	60.4	4.4		0.74	0.53	Na-HCO_3-Cl	-11.8	-84.9	0.70911	
72	7.8	12.0	4.4	170.0	4.6	0.55	357.0	54.0	44.0	1.8		0.65	0.60	Na-HCO_3	-11.7	-82.8	0.70879	
Upper Jurassic reservoir: Na-II																		
73	9.2	1.9	0.7	406.0	3.9	0.10	386.1	106.0	337.0	7.0		1.25	0.61	Na-SO4-HCO_3	-12.3	-87.7	0.70739	
74	7.8	18.3	10.8	208.0	6.9	1.20	338.0	11.0	236.0	5.6		0.84	0.97	Na-HCO_3-SO4	-11.2	-79.6	0.70766	
75	6.9	39.3	4.0	269.0	34.9	1.73	317.3	279.3	45.0		8.78	0.99	0.17	Na-Cl-HCO3	-10.5	-82.3	0.70951	10,9
76	6.6	96.8	14.8	738.7	54.2	4.02	477.5	870.3	93.8		15.8	2.35	0.25	Na-Cl-HCO3	-7.8	-75.0	0.70970	10,6
77	6.6	135.4	29.0	1853.6	85.2	6.40	854.2	2485.1	336.6	4.6	35	5.79	0.35	Na-Cl	-2.2	-60.6	0.70948	13,4
77	6.5	145.8	29.0	1857.1	64.8	6.40	779.0	2116.9	359.7			5.36	0.33	Na-Cl	-2.9	-60.7	0.70941	

Preprints (www.preprints.org) | NOT PEER-REVIEWED | Posted: 8 October 2022 doi:10.20944/preprints202210.0090.v1

No.	pH	Ca^{2+}	Mg^{2+}	Na^{+}	K^{+}	Sr^{2+}	HCO_3^{-}	Cl^{-}	SO_4^{2-}	F^{-}	B	TDS	Mg/Ca	Type	$\delta^{18}O$	δD	$^{87}Sr/^{86}Sr$	$\delta^{11}B$
	[-]	mg/l	mg/l	mg/l	mg/l	mg/l	mg/l	mg/l	mg/l	mg/l	mg/l	g/l	molar		‰	‰	[-]	‰
Upper Jurassic reservoir: Na-IV																		
78	7.2	15.1	4.5	316.3	20.9	0.66	552.0	166.5	5.6	10.0		1.09	0.49	Na-HCO_3-Cl	-10.6	-80.0	0.70944	
79	7.2	19.4	3.8	334.3	22.0	0.47	592.0	172.5	1.1	9.1		1.15	0.32	Na-HCO_3-Cl	-10.6	-79.9	0.70931	
80*	7.4	22.2	5.2	323.7	20.0	0.44	561.0	171.0	4.9	8.4		1.12	0.39	Na-HCO_3-Cl	-10.6	-79.8	0.70937	
81*	7.7	6.6	1.7	479.7	5.7	0.28	762.7	228.4	8.9	13.8		1.51	0.42	Na-HCO_3-Cl	-9.9	-73.4	0.70933	
82*	7.9	7.5	2.2	434.2	13.4	0.24	730.0	207.7		14.1		1.41	0.48	Na-HCO_3-Cl	-10.0	-75.2	0.70946	
83*	7.9	6.7	1.9	490.3	8.8	0.16	781.0	228.1	7.6	<3.1		1.52	0.46	Na-HCO_3-Cl	-9.5	-71.4	0.70888	
Upper Jurassic reservoir: Na-Va																		
84	7.5	32.7	7.0	385.9	17.9	0.94	393.6	404.7		6.0	1.26	1.25	0.35	Na-Cl-HCO_3	-10.7	-80.3	0.71843	11.2
85*	7.9	18.6	6.6	431.8	15.7	0.47	530.8	333.2				1.34	0.59	Na-Cl-HCO_3	-10.6	-77.5	0.71215	
Upper Jurassic reservoir: Na-Vb																		
86	8.2	33.3	18.6	151.9	17.9	0.86	457.6	93.7		0.7		0.77	0.92	Na-HCO_3-Cl	-11.4	-83.3	0.71016	
87	7.6	45.6	18.7	114.7	6.5	0.45	378.3	47.4	4.1	1.9		0.62	0.68	Na-Ca-HCO_3	-11.4	-83.2	0.70962	
88	7.6	45.7	19.7	125.2	15.4	0.53	408.8	67.8		0.8		0.68	0.71	Na-Ca-HCO_3-Cl	-11.4	-85.0	0.70916	

4.2. Hydrochemical and isotopic characterisation of the water samples

For hydrochemical and isotope analyses, groundwater samples from the Upper Jurassic as well as from overlying Tertiary formations were analysed. The results of these analyses are listed in **Table 3** and are described in the following section from top to bottom formation.

4.2.1. Water samples from the Cenozoic aquifer

The analysed waters from the topmost Cenozoic OSM aquifers originate from wells with depths up to 150 m bgl (below ground level) at the northern margin of the SGMB region. They are characterised in the Piper Plot (**Figure 5**a) as alkaline-earth bicarbonate Ca-(Mg)-HCO_3 type (field A) and have a low mineralisation (TDS 0.31 to 0.73 g/l). The stable hydrogen and oxygen isotope signatures (◎ ^{2}H: -81.3 to-65.5 ‰, ◎ ^{18}O: -11.3 to -9.3 ‰) scatter in **Figure 6**a along the Global Meteoric Water Line (GMWL) indicating infiltration of meteoric water during warm and cold climatic conditions. [87]. The investigated four water samples from the deeper aquifers of OMM, USM and UMM in the central SGMB highlight the broad hydrochemical variety (**Figure 5**a) of waters in deep Cenozoic formations [88]. The higher mineralised groundwaters with TDS ranging from 1.31 to 20.58 g/l are bicarbonate to chloride dominated alkaline waters (Na-HCO_3, Na-HCO_3-Cl or Na-Cl-HCO_3 type; field F and G) indicating considerable ion-exchange of Ca^{2+} by Na^{+}. The chloride contents may originate from influences of marine fossil formation waters in the host rocks (OMM and UMM). The stable hydrogen and oxygen isotope signatures show a common meteoric origin for samples 11 to 13 as both plot on the GMWL (**Figure 6**a). Only water sample 14 from the UMM indicates extensive secondary processes (evaporation, water-rock interaction) due to its position below the GWML, which is typical for fossil formation water in deep sedimentary basins [89,90].

4.2.2. Water sample from the Cretaceous aquifer

The groundwater sample 15 from the Cretaceous aquifer in the northeastern part of the SGMB shows ion-exchange processes of Ca^{2+} by Na^{+} and can therefore be classified as a Na-Ca-HCO_3-Cl water type. The mineralisation is relatively low with 0.64 g/l. The depleted stable water isotope signature of -84.9 ‰ for ◎ ^{2}H and -11.6 ‰ for ◎ ^{18}O plot on the GMWL (**Figure 6**a), which indicates cold climate recharge conditions [87].

4.2.3. Water samples from the Upper Jurassic aquifer

The hydrochemical and isotope composition of the groundwater samples from the Upper Jurassic aquifer are very heterogeneous due to the geographic distribution of the

Preprints (www.preprints.org) | NOT PEER-REVIEWED | Posted: 8 October 2022 doi:10.20944/preprints202210.0090.v1

samples and the varying depths of the reservoir. All groundwaters of the Upper Jurassic are in equilibrium with the carbonate host rocks.

The occurring groundwater types (Ca-(Mg)-HCO_3 to Na-Cl) can be classified by the dominant cation into calcium (Ca), including magnesium, and sodium (Na) dominated waters. The sub-classification (Ca-I to Ca-II) and (Na-Ia to Na-Vb) is based on their strontium isotope signature and the geographic location of the samples (**Table 3**).

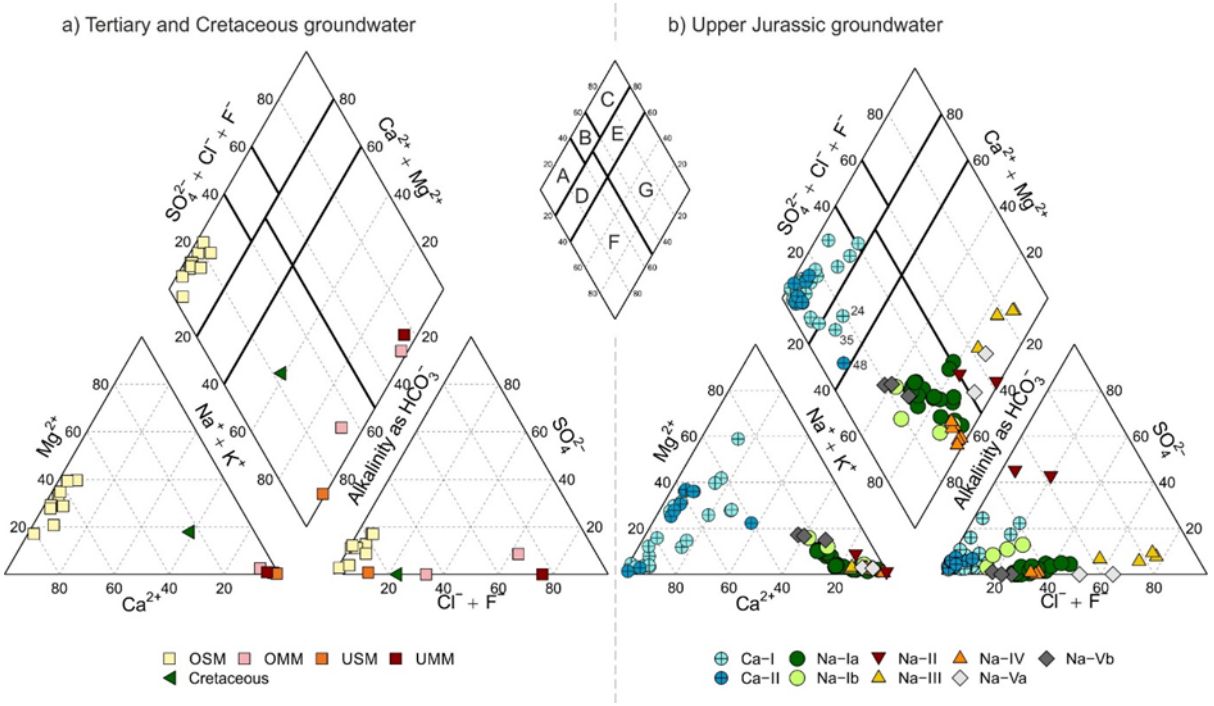

Figure 5. Hydrochemical characterisation with Piper Plots of the investigated samples from a) Tertiary and Cretaceous horizons and b) the Upper Jurassic aquifer. Classification system with fields A to F after Furtak & Langguth [91].

Ca-dominated waters

The calcium dominated Ca-I and Ca-II waters of the Upper Jurassic reservoir are predominantly from karst springs and shallow wells, with the exception of samples 35 and 48, which originate from deeper wells (> 215 m bgl). Their position in field A within the Piper Plot (**Figure 5**b) indicates mainly bicarbonate predominated alkaline-earth waters. The samples from the deeper wells 35 and 48 as well as the shallower well 24 with higher contents of sodium, instead plot in field D in the Piper Plot (**Figure 5**b) and, thus, indicate ion-exchange processes of Ca^{2+} by Na^{+}. Overall, the TDS of the Ca-dominated waters range between 0.33 to 0.63 g/l indicating low mineralisation. Overall, the stable water isotope values of -75.7 to -67.4 ‰ for $\delta^{2}H$ and -10.6 to -9.16 ‰ for $\delta^{18}O$ imply warm climate infiltration conditions [87]. Only water sample 48 clearly indicates cold climate recharge conditions with stable hydrogen and oxygen signatures of -89.4 ‰ for $\delta^{2}H$ and -12.5 ‰ for $\delta^{18}O$ (Figure 6b).

The hydrochemical composition and stable water isotope signatures of the karst springs and surface waters 39 and 41 are comparable to the calcium dominated shallow Upper Jurassic and even the shallow OSM groundwaters.

Na-dominated groundwaters

The sodium-dominated groundwaters of the Upper Jurassic are of complex nature and are therefore divided into five subgroups. The Na-I group with samples 51 to 69 (Na-Ia) and 70 to 72 (Na-Ib), are tapping the Upper Jurassic in greater depths between >600 up to 5000 m bgl and are used for (geo-) thermal energy production. These groundwaters highlight an ion-exchange character of Ca^{2+} by Na^{+} (**Figure 5**b), a low mineralisation (TDS

Preprints (www.preprints.org) | NOT PEER-REVIEWED | Posted: 8 October 2022 doi:10.20944/preprints202210.0090.v1

< 0.9 g/l) and stable hydrogen and oxygen isotope signatures with -90.4 to -83.9 ‰ for δ^2H and -12.6 to -10.6 ‰ for $\delta^{18}O$ (**Table 3**), indicating recharge within cold climatic conditions (**Figure 6**b). Slight isotopic enrichment and moderate chloride concentrations of several samples indicate limited mixing processes with Na-Cl containing formation waters [7,18,89].

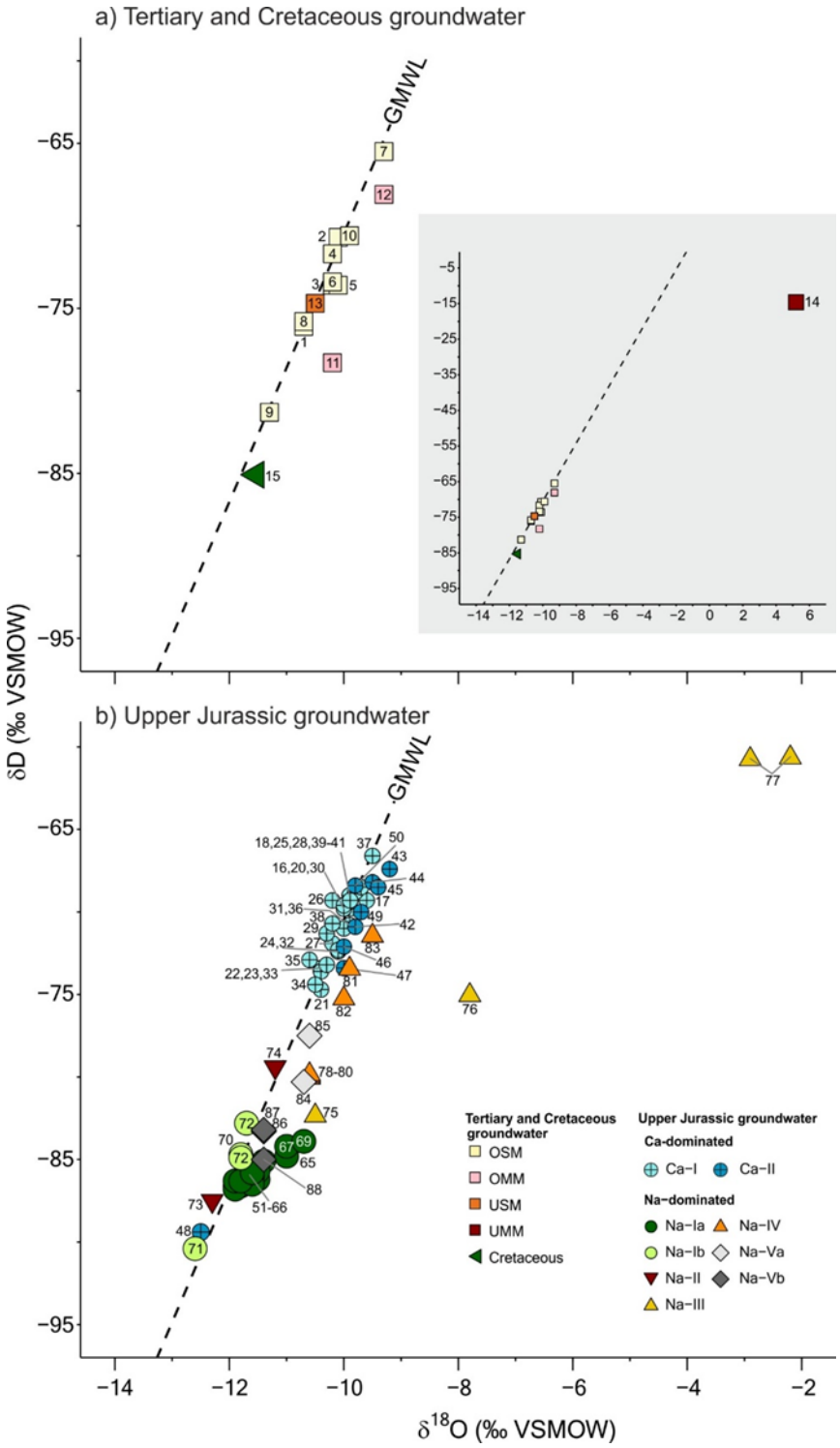

Figure 6. Plots of stable water isotopes of groundwater from a) Tertiary and Cretaceous aquifers and from the b) Upper Jurassic reservoir.

Preprints (www.preprints.org) | NOT PEER-REVIEWED | Posted: 8 October 2022 doi:10.20944/preprints202210.0090.v1

Samples 73 and 74 of the Na-II group are from the westernmost part of the SGMB. Similar to the groundwater of the Na-I group, these waters show meteoric signatures in the stable water isotopes (δ^2H: -87.7 to -79.6 ‰, $\delta^{18}O$: -12.3 to -11.2 ‰, **Table 3**), which also reflect cold climate recharge conditions [35]. They are characterised by strong ion-exchange processes of Ca^{2+} by Na^+. In contrast to Na-I groundwaters, these samples have a considerable amount of sulphate and an increased TDS of 0.84 and 1.25 g/l.

Higher mineralised groundwaters are found in samples 75 to 77 of the Na-III group, which originate from the central SGMB in the west and south-west of the greater Munich area. They are characterised by higher TDS (0.99 g/l to 5.79 g/l), Na-Cl domination (field G in Figure 5b) and elevated levels of DIC. The higher mineralisation (including DIC) and specific signatures of stable water isotopes, which plot below the GMWL (**Figure 6**b) with values between -82.3 to -60.6 ‰, for δ^2H and -10.5 to -2.24 ‰ for $\delta^{18}O$, suggest mixing with non-meteoric formation waters in contact to hydrocarbon reservoirs [89,90].

Wells with groundwaters of the Na-IV group (78 to 83) are tapping the Upper Jurassic reservoir in depths of maximum 2,000 m bgl within the so-called Braunauer Trog between the crystalline Landshut-Neuoetting High and Bohemian Massif. In comparison to Na-I groundwater samples these samples have an elevated TDS of 1.09 to 1.52 g/l due to higher levels of alkalinity, Na and Cl. They plot homogeneously distributed in field F of the Piper diagram and are consequently characterised by Na-HCO_3-Cl type (Figure 5b). The stable water isotope signatures of these thermal waters, show values between -80.0 to -71.4 ‰ for δ^2H and -10.6 to -9.94 ‰ for $\delta^{18}O$. They scatter below, but parallel to the GMWL, only indicating minor differences in the climatic conditions during recharge in this region. The distribution of these meteoric signatures does not suggest mixing with marine or saline formation water components.

In contrast to the relatively homogenous hydrochemical and stable water isotope composition of the thermal waters within the Braunauer Trog, different groundwaters of the Na-V group occur in the northwest of that area. These groundwaters can be further subdivided in two groups: Na-Va (samples 84 & 85) and Na-Vb (samples 86 to 88). Compared to Na-Vb and Na-IV (Field G, Figure 5b), the thermal groundwaters of Na-Va are characterised by significantly higher chloride contents with TDS values ranging from 1.25 to 1.34 g/L. The stable water isotope signatures (δ^2H: -80.3 and -77.5 ‰, $\delta^{18}O$: -10.7 and -10.6 ‰) are relatively similar to the groundwaters of Na-IV within the Braunauer Trog. Regarding Na-Vb waters, they have low contents of TDS (0.62 to 0.77 g/l) with a similar hydrochemical composition (field F, Figure 5b) and also comparable stable water isotope signatures (δ^2H: -85.0 to -83.3 ‰, $\delta^{18}O$: -11.4 ‰) to groundwaters of the Na-I group from the central SGMB (**Figure 6**b). The stable water isotope signatures also plot on the GMWL, implying recharge within cold climatic conditions.

4.3. Strontium isotopes as an indicator for specific water-rock interaction

Infiltrating meteoric water percolates through the soil zone and bedrock, where it dissolves strontium released by weathering of strontium-bearing minerals and controlled by the acid-carbonate-equilibrium. This process generates an initial $^{87}Sr/^{86}Sr$-signature in the groundwater. Further dissolution along the flow path can increase the basic strontium content and successively overprint the initial $^{87}Sr/^{86}Sr$ ratios [21,92–94]. These processes may also cause specific changes in the earth alkaline element (Ca^{2+}, Mg^{2+}, Sr^{2+}) composition. Since the $^{87}Sr/^{86}Sr$ ratio is not affected by isotope fractionation, the $^{87}Sr/^{86}Sr$ ratio can be used as a characteristic tracer for various strontium-bearing rock sources [21,92].

The strontium concentrations and $^{87}Sr/^{86}Sr$ ratios of all analysed groundwater samples in this study comprise a broad value range (**Figure 7**). As already described for the Upper Jurassic carbonate rocks of the SGMB, the specific $^{87}Sr/^{86}Sr$ signatures between 0.70706 and 0.70833 (**Table 3**, **Figure 3**), which are slightly above literature values of the paleo strontium seawater curve, have to be considered for the interpretation of the groundwater samples. In contrast, terrestrial silicate rocks, e.g. granites, clays or sandstones, are generally associated with much higher $^{87}Sr/^{86}Sr$ ratios than carbonates [92].

Preprints (www.preprints.org) | NOT PEER-REVIEWED | Posted: 8 October 2022 doi:10.20944/preprints202210.0090.v1

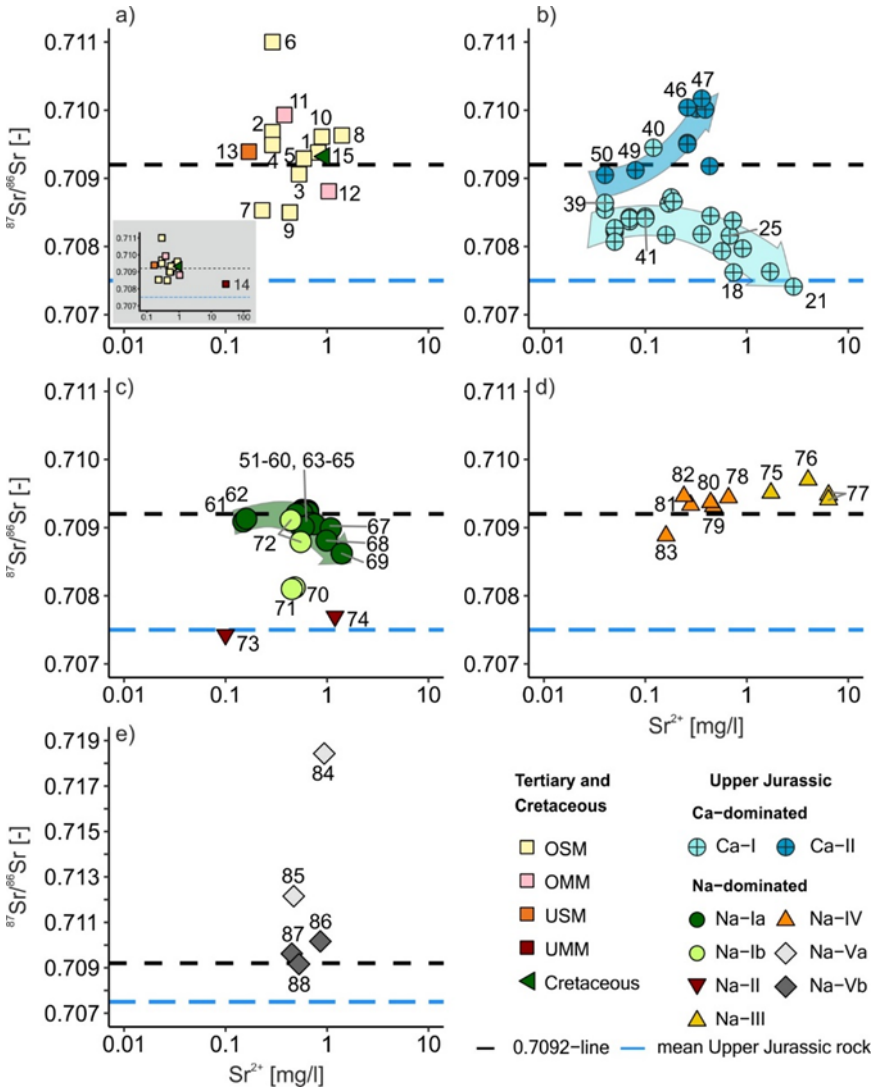

Figure 7. Plots of strontium isotope ratios vs. strontium content. Plot a) shows the signatures of groundwater from non-Upper Jurassic aquifers, b) to e) displays the signatures of different groundwater types from the Upper Jurassic reservoir.

4.3.1. Groundwater samples of the Cenozoic aquifer

The $^{87}Sr/^{86}Sr$ ratios of the groundwater samples from the fluviatile OSM (1 to 10) vary between 0.70853 and 0.71100 with strontium contents of 0.23 to 1.4 mg/l (**Figure 7**a). Nearly all samples are from the western region of the SGMB, showing no clear correlation of $^{87}Sr/^{86}Sr$ ratios with strontium contents. **Figure 8a** reveals a dependence of low to moderate Mg/Ca ratios (<0.4) with increasing $^{87}Sr/^{86}Sr$ values. It can be assumed, that groundwaters with varying strontium concentrations but low Mg/Ca ratios are unaltered and therefore indicate typical signatures of the soil zone. Ongoing water-rock interaction in this region have resulted in higher Mg/Ca ratios (>0.4) and approximately stable $^{87}Sr/^{86}Sr$ ratios of the groundwater samples (0.70938 and 0.70963). However, sample 6, from the deeper OSM in the north-eastern region of the SGMB, shows the highest Mg/Ca ratio (0.73), a very low strontium content (0.29 mg/l) and the most radiogenic $^{87}Sr/^{86}Sr$ signature (0.71100) within this group. This highlights considerable water-rock interactions with clastic host rocks that are most probably influenced by the crystalline rocks of the adjacent Bohemian Massif (**Figure 1**).

Preprints (www.preprints.org) | NOT PEER-REVIEWED | Posted: 8 October 2022 doi:10.20944/preprints202210.0090.v1

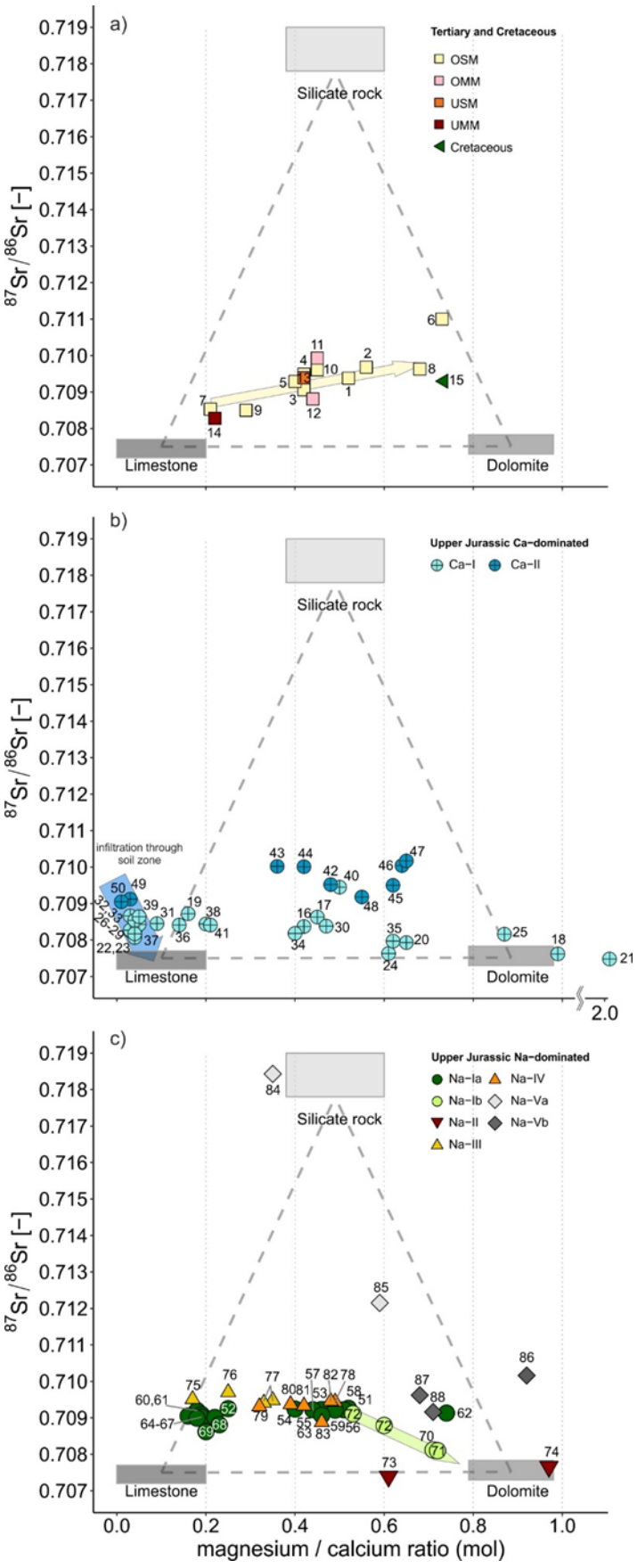

Figure 8. Plots of strontium isotope ratios vs. molar magnesium/calcium ratios with typical ranges of different rocks after [92]. a) shows the signatures of groundwater from non-Upper Jurassic aquifers and b) displays the signatures of different groundwater types from the Upper Jurassic reservoir.

Preprints (www.preprints.org) | NOT PEER-REVIEWED | Posted: 8 October 2022 doi:10.20944/preprints202210.0090.v1

Sample 13 from the fluviatile USM shows some radiogenic $^{87}Sr/^{86}Sr$ signature of 0.70939 with a low strontium concentration of 0.17 mg/l. The Mg/Ca ratio of 0.42 fits the systematic of the altered OSM samples (**Figure 7**a), suggesting considerable water-rock interaction with the terrestrial clastic host rocks.

Three samples of the Cenozoic marine aquifers were analysed from different parts of the SGMB. Two originate from the OMM, sample 11 and 12 with different $^{87}Sr/^{86}Sr$ values of 0.70993 and 0.70881, and sample 14 from the UMM with a $^{87}Sr/^{86}Sr$ value of 0.70828. The range of $^{87}Sr/^{86}Sr$ signatures for Cenozoic marine rocks derived from the Phanerozoic strontium seawater curve (**Figure 3**) are approximately between 0.7084 and 0.7086 for the OMM and between 0.7079 and 0.7082 for the UMM [79]. Sample 11 was obtained from the Braunauer Trog in the eastern part of the SGMB (**Figure 1**). This groundwater shows an elevated $^{87}Sr/^{86}Sr$ value compared to the typical seawater data. This is most likely due to detrital input of the nearby crystalline Bohemian Massif with elevated radiogenic $^{87}Sr/^{86}Sr$ signatures into the sedimentary UMM environment.

In contrast, the thermal water samples 12 (OMM) and 14 (UMM) from the central SGMB show relatively similar $^{87}Sr/^{86}Sr$ ratios in range of the corresponding seawater data [79]. This corresponding strontium isotope signature is remarkable, as both thermal groundwaters are of the same Na-Cl-HCO_3 type but show considerable differences in the Sr, Na and Cl contents, Sr/Cl ratios as well as the stable water isotope characteristics. This indicates that the $^{87}Sr/^{86}Sr$ ratios are independent of groundwater mineralisation or mixing processes with non-meteoric formation water and only relate to equilibration with the marine host rock.

In conclusion, the results of the investigated groundwater samples from the Cenozoic aquifer imply that the strontium isotope fingerprint is driven by water-rock-interaction with the host rock as part of the geochemical evolution.

4.3.2. Groundwater sample of the Cretaceous aquifer

The $^{87}Sr/^{86}Sr$ ratio of sample 15 (0.70932) is above the typical range for marine Cretaceous sediments derived from the Phanerozoic strontium seawater curve (<0.708) [79]. This, in relation to the Na-Ca-HCO_3-Cl water type indicating incomplete ion exchange processes, implies a terrigenous host sediment for the rock-water interaction. Moreover, the expected recharge within cold climatic conditions also suggests transformational fluid migration of this groundwater.

4.3.3. Groundwater samples of the Upper Jurassic aquifer

Ca-dominated waters

The calcium dominated Upper Jurassic groundwaters show considerable variations of strontium contents and its isotope signatures (**Figure 7**b). The $^{87}Sr/^{86}Sr$ ratios between 0.70841 and 0.70945 of samples 39 to 41, derived from surface and spring waters, may represent a plausible range for weathering and strontium uptake processes in the soil zone in this region [93]. The strontium isotope signatures of most Ca-I and Ca-II groundwaters with low strontium concentrations (<0.1 mg/l) and accordingly Mg/Ca ratios near zero are consistent with this range.

The samples 22, 23, 26 and 27 with lower $^{87}Sr/^{86}Sr$ signatures and low strontium concentrations as well as decreased Mg/Ca ratios <0.05, originate from the exposed Upper Jurassic karst [35]. This may indicate higher influences of easily dissolvable marine calcitic carbonates. Comparable $^{87}Sr/^{86}Sr$ ratios were found in Upper Jurassic groundwaters of the Steinheim basin, which are also from the exposed Upper Jurassic rocks of the Swabian Alb [95].

With increasing strontium content and higher Mg/Ca ratios, two different trends of $^{87}Sr/^{86}Sr$ values can be observed (**Figure 7**b). The increased Mg/Ca ratios imply that strontium uptake occurs not only by easily soluble calcites but also by magnesium rich minerals. Several Ca-I groundwaters show a trend with increasing strontium content to lower $^{87}Sr/^{86}Sr$ ratios from 0.70872 (Sr^{2+} 0.18 mg/l) down to 0.70741 (Sr^{2+} 2.9 mg/l), which indicates ongoing water-rock interaction processes with the Upper Jurassic reservoir rocks.

Preprints (www.preprints.org) | NOT PEER-REVIEWED | Posted: 8 October 2022 doi:10.20944/preprints202210.0090.v1

In contrast, Ca-II groundwaters tend to higher, radiogenic $^{87}Sr/^{86}Sr$ ratios with increasing strontium concentrations, implying water-rock interaction with terrestrial sediments most probably eroded from the Bohemian massif. Therefore, a considerable influence of the overlying Tertiary sandy freshwater molasse sediments may be deduced. Conclusively, an interacting aquifer system with transformational flow from the Tertiary to the Upper Jurassic aquifer in the vicinity of the Danube drainage system is very likely in the northern part of the SGMB (Figure 8).

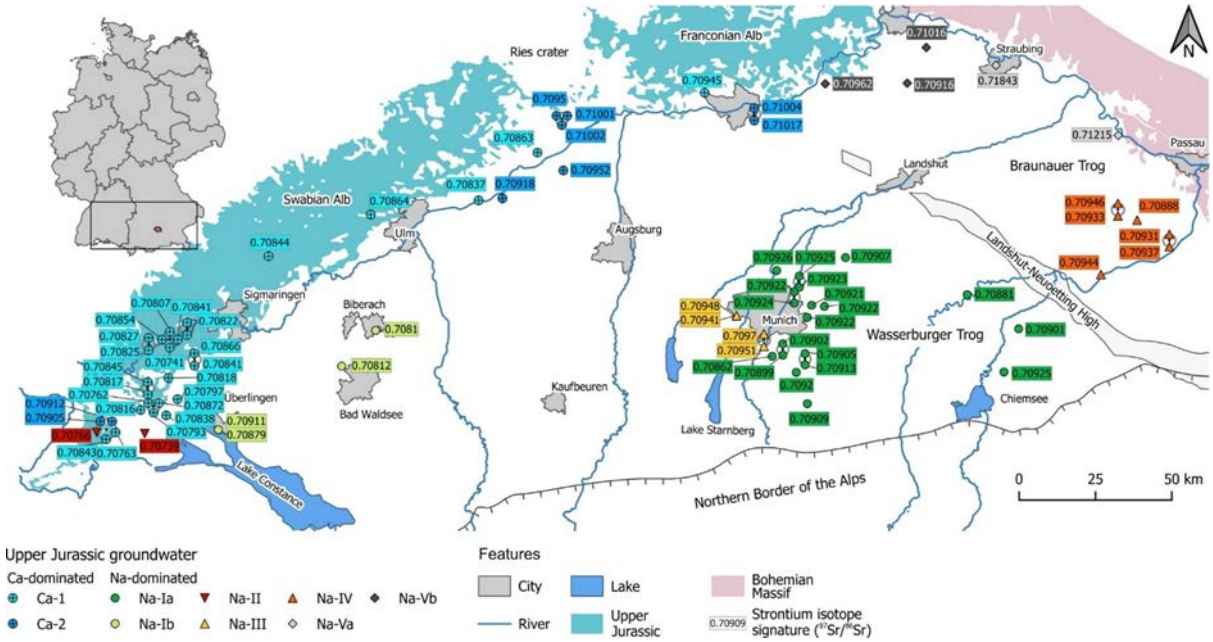

Figure 8. Results of $^{87}Sr/^{86}Sr$ ratios of Upper Jurassic groundwaters in the SGMB.

Na-dominated groundwaters

The Na-Ia groundwaters in the central SGMB originate from wells with depths between 1800 and 5000 m bgl. Their $^{87}Sr/^{86}Sr$ values show a broad range from 0.70862 (69) to 0.70926 (51) (**Figure 7**c). Most of the Na-Ia groundwaters with strontium contents below 0.65 mg/l only reveal minor variations of the $^{87}Sr/^{86}Sr$ ratios between 0.70913 and 0.70926 while heterogeneous Mg/Ca ratios are ranging from 0.2 to 0.7. Such low strontium contents and simultaneous high radiogenic $^{87}Sr/^{86}Sr$ ratios are untypical for groundwaters associated with significant water-rock interaction with the marine Upper Jurassic host rocks and suggest initial interaction with terrestrial formations. However, some Na-Ia groundwaters with increasing strontium contents up to 1.44 mg/l, show a trend to considerably lower $^{87}Sr/^{86}Sr$ values down to 0.70862. Additionally, their low Mg/Ca ratios (around 0.2) suggest calcium uptake from easily dissolvable calcite, which also serves as a secondary source of strontium for these Na-Ia waters (**Figure 8)**. Therefore, higher strontium contents indicate considerable influences of interactions between the groundwater and the hosting Upper Jurassic carbonates, which are characterised by significantly lower $^{87}Sr/^{86}Sr$ ratios (**Figure 3**). In summary, the Na-Ia groundwaters show a tendency of increasing strontium uptake from the Upper Jurassic carbonate rocks with a shift of the heterogeneous Mg/Ca ratios to uniform values of around 0.2 indicating preferential influence of calcite (**Figure 8b**). However, the characteristic signature of the Upper Jurassic marine rock is not reached (**Figure 7**c) and the radiogenic influence is still present in these groundwater samples.

The $^{87}Sr/^{86}Sr$ values of the Na-Ib groundwaters (70-72) in the western SGMB, north of Lake Constance (Figure 8), vary between 0.70810 and 0.70911. Compared to the Upper Jurassic host rocks, their slight radiogenic $^{87}Sr/^{86}Sr$ ratios indicate water-rock interaction with terrestrial formations. The $^{87}Sr/^{86}Sr$ signatures are generally lower than for most of

Preprints (www.preprints.org) | NOT PEER-REVIEWED | Posted: 8 October 2022 doi:10.20944/preprints202210.0090.v1

the Na-Ia groundwaters and show no dependence on strontium content (0.45 to 0.55 mg/l), but instead a correlation with the Mg/Ca ratio (**Figure 8**). As the Mg/Ca ratio increases (from 0.53 to 0.72), the $^{87}Sr/^{86}Sr$ values decrease and approach the Upper Jurassic carbonate signatures. This may be explained by the influence of dissolution of carbonates from the water-bearing and dolomite-rich Lochfels formation in this area of the SGMB [46].

The $^{87}Sr/^{86}Sr$ ratios (0.70766 and 0.70739) of groundwater samples 73 and 74 from the Na-II group represent typical values for the Upper Jurassic carbonates as described herein. The strontium contents (0.1 and 1.2 mg/l) and Mg/Ca ratios (0.61 and 0.99) of both samples differ and do not follow a clear systematic in relation to the $^{87}Sr/^{86}Sr$ signatures. Considering the high sulphate contents, these waters point to an initial dissolution of evaporitic rocks. Therefore, their $^{87}Sr/^{86}Sr$ signatures may also be influenced by interaction with the underlying marine Muschelkalk formation [35,96].

Groundwaters of the Na-III group (samples 75 to 77) occur in the western vicinity of the Na-Ia group in the central SGMB (**Figure 8**). They are characterised by varying hydrochemical and stable water isotope composition similar to groundwaters of Na-I and Na-II. In addition, the strontium contents (1.73 to 6.40 mg/l) and radiogenic $^{87}Sr/^{86}Sr$ ratios (0.70941 to 0.70970) of these deep groundwater samples are considerably elevated (**Figure 7**). In contrast to the Na-I and Na-II groundwaters, the increased strontium contents cannot be attributed to a strontium uptake from the Upper Jurassic carbonates due to very high $^{87}Sr/^{86}Sr$ ratios. The minor variation of the $^{87}Sr/^{86}Sr$ values of these samples neither correlate with the strontium content nor the Mg/Ca ratio (**Figure 7**d & **Figure 8c**). These groundwaters show the highest gas contents (CO_2 and CH_4) of Upper Jurassic groundwater in the SGMB [4,97]. Thus, the missing correlations may be related to degradation of hydrocarbons, resulting in CH_4 and CO_2 generation, which is also recognisable in elevated levels of alkalinity (**Table 3**). Depending on the CO_2 content caused by this degradation, both calcitic and dolomitic minerals can be dissolved, which leads to different Mg/Ca ratios of these samples (**Figure 8**). In conclusion, the radiogenic $^{87}Sr/^{86}Sr$ signatures of the Na-II groundwater samples strongly indicate water-rock interactions in terrestrially influenced sediments.

The $^{87}Sr/^{86}Sr$ values of Na-IV (78-83) groundwaters in the Braunauer Trog range between 0.70888 and 0.70946 with strontium contents from 0.16 to 0.66 mg/l. Despite slightly different recharge conditions, indicated by the stable water isotope signatures (**Figure 6**b) and varying TDS values, these groundwaters are all dominated by radiogenic strontium input. The $^{87}Sr/^{86}Sr$ signatures of samples 78 to 82 are independent of the strontium, calcium and magnesium content, the Mg/Ca ratio, as well as the chloride content (**Figure 7**d, **Figure 8c** & **Table 3**). Compared to the samples of the Na-I group, the highly alkaline groundwaters imply processes of CO_2 generation in the Braunauer Trog. These processes apparently have resulted in homogeneous Mg/Ca ratios with very low earth-alkaline contents, including strontium. As groundwaters with low strontium contents may easily be affected by strontium dissolution from aquifer rock material or mixing with other fluids, the radiogenic $^{87}Sr/^{86}Sr$ ratios of these samples suggest influences by eroded terrestrial rock material most likely from the nearby crystalline Bohemian Massif (**Figure 8**). Only sample 83 with a minimum $^{87}Sr/^{86}Sr$ ratio (0.70888) and strontium content (0.16 mg/l) may be influenced by water-rock interaction with marine carbonates, presumably of the Upper Jurassic host rocks.

The wells of group Na-Va (84 and 85) are located at the north-eastern margin of the SGMB in proximity to the crystalline Bohemian Massif. The significantly high $^{87}Sr/^{86}Sr$ ratios of 0.71215 and 0.71843 show no dependency to the strontium contents of 0.47 and 0.94 mg/l (**Figure 7**e). A considerable influence of water-rock interaction with silicate rocks such as crystalline rocks (e.g. granites) [8,9] of the Bohemian Massif or their erosive sediments in the local Tertiary formations, is indicated by the radiogenic $^{87}Sr/^{86}Sr$ values of the Na-Va groundwaters. A slight tendency of increasing $^{87}Sr/^{86}Sr$ signatures and decreasing Mg/Ca ratios can be recognized (**Figure 8c**) with a likely dependence on higher chloride

 doi:10.20944/preprints202210.0090.v1

contents (**Table 3**). Although these thermal waters appear to be recharged in different climatic periods (**Figure 6**b), no significant water-rock interaction with carbonates of the Upper Jurassic aquifer is evident. Therefore, an influence of transformational groundwater from aquifer systems with radiogenic $^{87}Sr/^{86}Sr$ ratios seems reasonable.

The three wells (86 to 88) of Na-Vb group are located in close proximity and to the west of the Na-Va groundwaters and can be distinguished by slightly lower radiogenic $^{87}Sr/^{86}Sr$ ratios (0.70916 to 0.71016). Their stable water isotope fingerprint and hydrochemical characteristics are consistent, but strontium contents (0.45 to 0.86 mg/l) and Mg/Ca ratios (between 0.68 and 0.92) (**Figure 8c**) differ notably. The radiogenic $^{87}Sr/^{86}Sr$ ratios of the samples do not indicate considerable water-rock interaction with the Upper Jurassic carbonates. In contrast to the Na-Va groundwaters, the $^{87}Sr/^{86}Sr$ ratios do not reveal a clear correlation to the chloride contents. However, as well 86 is located in a fault system [98], the groundwater sample is most likely influenced by transformation groundwaters due to its relatively high $^{87}Sr/^{86}Sr$ ratio of 0.71016 and elevated chloride concentration (93.7 mg/l) and is thus comparable to those of the Na-Va group.

4.4. Boron isotopes as an indicator for specific water-rock interaction

Although the nine samples from geothermal wells in the SGMB are differentiated in three Na-dominated groundwater groups (Na-Ia, Na-III and Na-Va), their $\delta^{11}B$ values comprise a relatively narrow range from 8.6 to 13.4 ‰ (**Table 3** & **Figure 9**). They coincide with the upper range of the $\delta^{11}B$ values from the Upper Jurassic marine carbonates (**Figure 4**) and show no trend towards boron concentrations (0.7 to 35.0 mg/l) (**Figure 9**a). However, samples of the Na-Ia and Na-Va group reveal lower boron concentrations (0.7 to 3.3 mg/l) compared to the Na-III group with higher boron concentrations (8.8 to 35.0 mg/l) and the maximum $\delta^{11}B$ value of up to 13.4 ‰. Interestingly, the Na-Ia and Na-III samples demonstrate a correlation of the $\delta^{11}B$ values with increasing $^{87}Sr/^{86}Sr$ ratios (**Figure 8b**). In contrast to the radiogenic $^{87}Sr/^{86}Sr$ ratios indicating terrestrial influence, the higher $\delta^{11}B$ signatures imply an influence of marine imprinted host rocks [99]. Since the difference between the $\delta^{11}B$ signatures of Tertiary (37.5 to 39.5 ‰) and Upper Jurassic seawater (39.0 to 41.5 ‰) is relatively small, boron isotope fractionation for carbonates [39] results in nearly equivalent $\delta^{11}B$ signatures of the Tertiary marine carbonate material (Figure 4). The strontium-boron-isotope-correlation of the groundwater samples indicate an influence of marine-formed but terrestrially influenced Tertiary sediments. Therefore, $\delta^{11}B$ values of these water samples may also be affected by marine carbonate material of the Tertiary in the SGMB, which agree with their higher $^{87}Sr/^{86}Sr$ signatures and with the overall picture of the recharge systematic of the Upper Jurassic groundwater in the central SGMB [18,60].

The $\delta^{11}B$ signature of sample 84, in the north-east of the SGMB, seems to represent a similar process to that observed for samples from the central SGMB. Although, the very radiogenic $^{87}Sr/^{86}Sr$ ratio (0.71843) may indicate water-rock interaction with crystalline rocks of the adjacent Bohemian Massif, the relatively high $\delta^{11}B$ signature of 11.2 ‰ specifies a marine origin for the very low boron concentration (1.3 mg/l). This implies a considerable influence of the marine Tertiary sediments, which comprise eroded material from the Bohemian Massif.

Preprints (www.preprints.org) | NOT PEER-REVIEWED | Posted: 8 October 2022 doi:10.20944/preprints202210.0090.v1

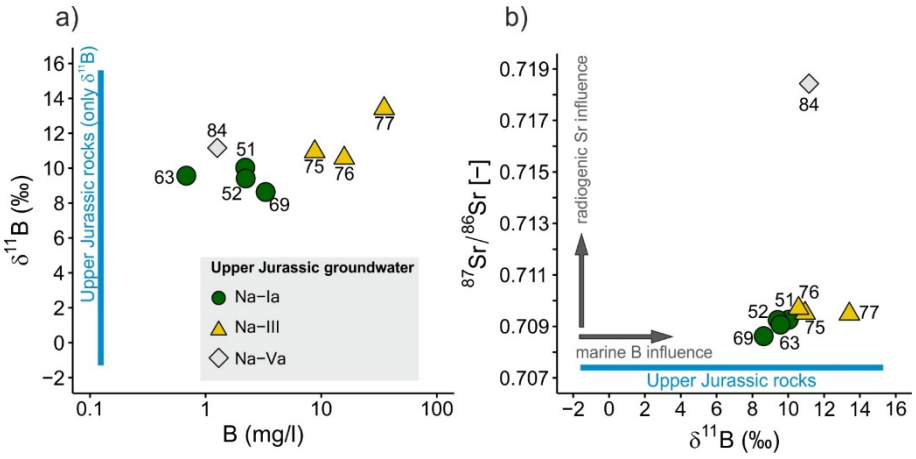

Figure 9. Plots of a) boron isotopes and boron concentration and b) boron isotopes vs. strontium isotopes. The values for Upper Jurassic rocks originate from this study.

4.5. Synthesis of the hydrogeochemical evolution of the groundwaters in the Upper Jurassic aquifer

Based on strontium and boron isotope data of the Upper Jurassic groundwaters, the interpretation of their hydrogeochemical composition and evolution is synthesised in comparison to the geogenic isotope signatures of the Upper Jurassic rock samples.

The results of $^{87}Sr/^{86}Sr$ and ◎ ^{11}B analyses of the Upper Jurassic carbonates show deviations from the expected values for marine carbonates of this formation. The $^{87}Sr/^{86}Sr$ ratios of the investigated Upper Jurassic rock samples are slightly elevated compared to the typical signatures of the Upper Jurassic seawater [34,78,79], which may be explained by an input of eroded terrestrial material from the crystalline Bohemian Massif during sedimentation.

The hydrogeochemical composition of current groundwaters in the Upper Jurassic carbonates shows a broad variety due to different water-rock interaction processes in the western, northern, central and eastern SGMB, which will be summarised in the following.

4.5.1. Western and northern SGMB

The calcium dominated Upper Jurassic groundwaters at the western and northern margins of the SGMB show two main mechanisms of hydrochemical maturation after equilibration within the soil zone. The $^{87}Sr/^{86}Sr$ ratios of Ca-I groundwaters approach the typical signature of the marine carbonates with increasing strontium contents, implying interaction with the Upper Jurassic carbonates. In contrast, the Ca-II groundwaters show rather radiogenic $^{87}Sr/^{86}Sr$ ratios with increasing strontium contents, similar to the trend of the OSM-groundwaters. For the Ca-II groundwaters this indicates influences of water-rock interaction with sediments that are characterised by radiogenic $^{87}Sr/^{86}Sr$ signatures.

The Ca-II groundwaters predominantly occur at the north-western and north-central margin of the SGMB. Therefore, the $^{87}Sr/^{86}Sr$ ratios of Ca-II group indicate a hydraulic connection to the overlying Tertiary terrestrial sediment cover.

Sodium dominated groundwaters of the Na-Ib and Na-II group in this area (**Figure 1**) reveal ion-exchange processes, which cannot be related to the exchange with Upper Jurassic carbonates. The thermal Na-Ib waters show a hydrochemical maturation, in contrast to the Ca-dominated groundwaters in their vicinity. In addition, the radiogenic $^{87}Sr/^{86}Sr$ ratios of these groundwaters indicate water-rock interaction with terrestrial rocks. With increasing magnesium content, the $^{87}Sr/^{86}Sr$ signatures decrease presumably due to interaction with the dolomite-rich Upper Jurassic rocks. In contrast, the Na-II groundwaters with low $^{87}Sr/^{86}Sr$ ratios and high sulphate contents indicate an evaporitic influence, most likely from the deeper Muschelkalk aquifer.

4.5.2. Central SGMB

 doi:10.20944/preprints202210.0090.v1

In this deep part of the carbonate aquifer, calcium dominated groundwaters are not present.

Meanwhile, Na-Ia groundwaters prevail in the Upper Jurassic geothermal system of the central SGMB. Their hydrochemical composition cannot be explained by a hydrogeochemical evolution within the carbonate aquifer from the calcium dominated Ca-I and Ca-II groundwaters at the northern margins of the SGMB. Na-Ia groundwaters therefore require a specific hydrochemical evolution due to their ion-exchange character. Furthermore, their $^{87}Sr/^{86}Sr$ signatures indicate only minor interaction with the Upper Jurassic host rocks as the groundwaters are characterised by considerable radiogenic $^{87}Sr/^{86}Sr$ ratios. They imply an uptake of rather radiogenic strontium in the overlying Tertiary sediments. Only few samples show an approximation to lower $^{87}Sr/^{86}Sr$ ratios with increasing strontium contents, which can be explained by minor subsequent dissolution of Upper Jurassic carbonates. As Na-Ia groundwaters have been recharged within cold climate conditions during the last glaciations [18,60], this strongly supports the concept of transformational infiltration of the overlying Tertiary formations into the Upper Jurassic in the areas of the glaciations. Thus, the radiogenic $^{87}Sr/^{86}Sr$ signatures and ion-exchange character resulted from this infiltration process by the interaction with Tertiary sediments.

The process of transformational infiltration may also be visible in the Upper Jurassic vein calcite samples, as GV1 and GV3 of the GEN drill core in the southern central SGMB show comparable radiogenic $^{87}Sr/^{86}Sr$ ratios to the Na-Ia group. This is in agreement with the salinity of fluid inclusions and stable isotope composition of the vein calcites GV1 and GV2 as described in [41] and confirmed by $\delta^{13}C\text{-}CaCO_3$ and $\delta^{18}O\text{-}CaCO_3$ values within this study (**Table 2**). Moreover, the stable isotope composition of the vein calcites may indicate formation temperatures that are too low for the burial depth of the Upper Jurassic.

Higher saline Na-III groundwaters occur in direct vicinity to the west of the Na-Ia group and show considerably higher strontium contents and even higher radiogenic $^{87}Sr/^{86}Sr$ values. Their hydrogeochemical and isotope composition indicate an ongoing hydraulic connection to overlying Tertiary rocks and mixing with their non-meteoric formation waters [18]. Due to these significant differences in the hydrogeochemical composition of Na-Ia and Na-III groundwaters, a direct inflow of non-meteoric high saline Tertiary formation water is not observable to the same extend for the Na-Ia groundwaters.

4.5.3. Eastern SGMB

The Na-IV groundwaters in the Braunauer Trog are characterised by higher mineralisation with no evidence of explicit cold climate recharge conditions compared to Na-I and Na-II groundwaters. Meanwhile, these groundwaters show a high degree of hydrogeochemical maturation, suggesting distinct and complex hydrogeological systematics in this area. Based on the $^{87}Sr/^{86}Sr$ signatures with a considerable radiogenic influence, only one Upper Jurassic groundwater sample (well 83) reveals water-rock interaction with the aquifer carbonates. In addition, the hydrogeochemical evolution and $^{87}Sr/^{86}Sr$ ratio of sample 11 from the OMM are very similar to the general hydrochemical characteristics of the Na-IV group. This agrees with the hypothesis of an overall hydraulic interaction between the overlying Tertiary formations and the Upper Jurassic aquifer [8,9]. Since the derived apparent ^{81}Kr model ages are very high (approximately 500,000 years) [60] and cold climate recharge effects are negligible, this hydraulic interaction dynamic seems to be relatively slow.

At the northern margin of the Braunauer Trog in vicinity of the Bohemian Massif, the occurring Na-Va groundwaters show higher mineralisation, predominantly caused by considerable NaCl contents, and contain even more radiogenic strontium than Na-IV groundwaters. An influence of deep circulating ascending crystalline waters [63] in proximity of the Danube drainage system may be a plausible explanation, however the boron isotope data indicate fingerprinting by marine Tertiary sediments of the SGMB in this region. This influence gradually diminishes towards the west, where the Upper Jurassic

groundwater is represented by lower mineralisation of the Na-Vb group. They are characterised by cold climate recharge conditions and less radiogenic strontium. Therefore, Na-Vb groundwaters show a significant influence of Na-Ia groundwaters due to the comparable hydrochemical and isotope characteristic. Accordingly, the assumption of a flow direction from the central SGMB towards the north of the Danube drainage system is supported [8,9,11,18].

5. Conclusions

The here presented hydrochemical groundwater and rock data from the SGMB contribute to an improved understanding of the groundwater recharge mechanism in the deep and heterogeneous carbonate aquifer system of the Upper Jurassic in the SGMB. Groundwaters in the Upper Jurassic carbonates highlight a specific evolution in the foreland basin of an orogeny. In particular the geothermal exploration and utilisation have revealed a widespread distribution of homogeneously low mineralised groundwater with ion exchange character in the central SGMB between Munich and the LNH. These groundwaters differ considerably in hydrochemical and isotope composition from groundwaters in the western, northern, and eastern parts of the aquifer. Isotope analyses of these groundwaters indicated recharge during latest cold climate conditions in the southern area of the SGMB, where widespread glaciation occurred. The comprehensive strontium isotope survey, supplemented with boron isotope investigations, confirms the transformational recharge of groundwater into the deeply buried Upper Jurassic aquifer. These groundwaters still represent the hydrogeochemical maturation and isotope fingerprint of the overlying Tertiary Molasse formations. In particular, the radiogenic $^{87}Sr/^{86}Sr$ signatures of the thermal groundwaters in the central SGMB clearly document the differences of Upper Jurassic carbonates and the groundwaters towards the margins of the basin. The groundwaters in vicinity of the central SGMB have distinct hydrochemical and isotope fingerprints due to specific regional hydro-geological conditions. Here, a similar transformational flow can also be observed, however due to the missing glacial influence these processes appear slower.

Author Contributions: "Conceptualization, J.S., F.H. and M.H.; methodology, F.H., J.S. and M.H.; software, F.H.; validation, M.H. and M.R.; formal analysis, F.H. and M.R..; investigation, J.S. and F.H.; data curation, F.H.; writing—original draft preparation, J.S. and F.H.; writing—review and editing, J.S., F.H., M.H. and M.R.; visualization, F.H.; supervision, M.H..; project administration, F.H.; funding acquisition, J.S. and F.H. All authors have read and agreed to the published version of the manuscript."

Funding: "This work was performed in the framework of the project IsoMol (grant number FKZ 104-0270-88806/2016, 104-0270-16955/2017), which was funded by the Bavarian State Ministry of the Environment and Consumer Protection (StMUV), the project Geothermal-Alliance Bavaria (GAB), which was funded by the Bavarian Ministry of Science and Art (StMWK) and the project Dolomitkluft (grant number 0324004 B), which was funded by the Federal Ministry for Economic Affairs and Energy (BMWi) on the basis of a decision by the German Bundestag [0324004]. The APC was funded by Hydrosion GmbH."

Data Availability Statement: "All data used are reported in the article."

Acknowledgments: "The authors wish to thank Dr. Thomas Fritzer and Dr. Timo Spörlein from the Bavarian Environmental Agency (Bayerisches Landesamt für Umwelt, LfU) and Dr. Christoph Töpfner from the Bavarian Ministry for Environment as well as Dr. Florian Einsiedl (Chair of Hydrogeology, TUM) for initiating, supporting and guiding the IsoMol project. The authors thank Susanne Thiemann who was involved in analysing hydrochemical data and stable water isotopes at the laboratory of TUM, Chair of Hydrogeology as well as Daniel Bohnsack (Chair of Hydrogeology, TUM) and Elena Mraz (Chair of Engineering Geology, TUM) for providing some rock samples. Moreover, we thank Hydroisotop GmbH for additional analyses as well as Dr. Lena Kölbel and Rachel McRae of Hydrosion GmbH for their support and proof reading. Special thanks go to all owners of the investigated wells as well as geothermal and balneological sites for having the opportunity to sample."

 doi:10.20944/preprints202210.0090.v1

Conflicts of Interest: "The authors declare no conflict of interest."

References

[1] T. Agemar, J.-A. Alten, B. Ganz, J. Kuder, K. Kühne, S. Schumacher, R. Schulz, The Geothermal Information System for Germany – GeotIS, Z. Dt. Ges. Geowiss. (German J. Geosci.). 165 (2014) 129–144. https://doi.org/10.1127/1860-1804/2014/0060.

[2] K. Lemcke, W. Tunn, Tiefenwasser in der süddeutschen Molasse und ihrer verkarsteten Malmunterlage, Bull. Ver. Schweiz. Pet. u. -Ing. 23 (1956) 35–56.

[3] P. Udluft, Das tiefere Grundwasser zwischen Vindelicischem Rücken und Alpenrand, Geol. Jahrb. C11 (1975) 3–29.

[4] C. Mayrhofer, R. Niessner, T. Baumann, Hydrochemistry and hydrogen sulfide generating processes in the Malm aquifer, Bavarian Molasse Basin, Germany, Hydrogeol. J. 22 (2014) 151–162. https://doi.org/10.1007/s10040-013-1064-2.

[5] I. Stober, Hydrochemical properties of deep carbonate aquifers in the SW German Molasse basin, Geotherm. Energy. 2 (2014) 13. https://doi.org/10.1186/s40517-014-0013-1.

[6] K. Lemcke, Übertiefe Grundwässer im süddeutschen Alpenvorland, Bull. Ver. Schweiz. Pet. u. -Ing. 42 (1976) 9–18.

[7] W. Stichler, W. Rauert, S. Weise, M. Wolf, G. Koschel, P. Stier, R. Prestel, K. Hedin, B. Bertleff, Isotopenhydrologische und hydrochemische Untersuchungen zur Erkundung des Fließsystems im Malmkarstaquifer des süddeutschen Alpenvorlandes., Z. Dt. Geol. Ges. 138 (1987) 387–398.

[8] R. Prestel, Hydrochemische Untersuchungen im süddeutschen Molassebecken, in: H. Frisch, J. Werner (Eds.), Schlussbericht Forschungsvorhaben 03 E 6240 A/B Hydrogeothermische Energiebilanz Und Grundwasserhaushalt Des Malmkarstes Im Süddeutschen Molassebecken, 1991, Bayerisches Landesamt für Wasserwirtschaft, Geologisches Landesamt Baden-Württemberg, 1988: p. 64.

[9] S. Weise, M. Wolf, P. Fritz, W. Rauert, W. Stichler, R. Prestel, B. Bertleff, M. Stute, Isotopenhydrologische Untersuchungen im Süddeutschen Molassebecken, in: H. Frisch, J. Werner (Eds.), Schlussbericht Forschungsvorhaben 03 E 6240 A/B Hydrogeothermische Energiebilanz Und Grundwasserhaushalt Des Malmkarstes Im Süddeutschen Molassebecken, 1991, Bayerisches Landesamt für Wasserwirtschaft, Geologisches Landesamt Baden-Württemberg, München, Freiburg i.Br., 1991: p. 106.

[10] B. Bertleff, D. Ellwanger, C. Szenkler, L. Eichinger, P. Trimborn, N. Wolfendale, Interpretation of hydrochemical and hydroisotopical measurements on palaeogroundwaters in Oberschwaben, south German alpine foreland, with focus on quaternary geology, in: Int. At. Energy Agency, International Atomic Energy Agency, Vienna, Austria, 1993: pp. 337–357.

[11] H. Frisch, B. Huber, Ein hydrogeologisches Modell und der Versuch einer Bilanzierung des Thermalwasservorkommens im Malmkarst des süddeutschen Molassebeckens., Hydrogeol. Und Umwelt. 20 (2000) 25–43.

[12] B. Bertleff, R. Watzel, Tiefe Aquifersysteme im südwestdeutschen Molassebecken. Eine umfassende hydrogeologische Analyse als Grundlage eines zukünftigen Quantitäts- und Qualitätsmanagements, Abh. Geol. Landesamt Baden-Württemb. 15 (2002) 75–90.

[13] J. Birner, C. Mayr, L. Thomas, M. Schneider, T. Baumann, A. Winkler, Hydrochemie und Genese der tiefen Grundwässer des Malmaquifers im bayerischen Teil des süddeutschen Molassebeckens., Z. Geol. Wiss. 39 (2011) 291–308.

[14] G. Andres, H. Frisch, Hydrogeologie und Hydraulik im Malmkarst des Molassebeckens und der angrenzenden Fränkisch-Schwäbischen Alb, in: G. Andres, H. Wirth (Eds.), Die Therm. Und Schwefelwasservorkommen von

Bad Gögging, Schriftenreihe Bayerisches Landesamt für Wasserwirtschaft, München, 1981: pp. 108–117.

[15] L. Kiraly, Projekt Malmkarst: Programmbeschreibung zum Grundwasserströmungsmodell, in: H. Frisch, J. Werner (Eds.), Schlussbericht Forschungsvorhaben 03 E 6240 A/B Hydrogeothermische Energiebilanz Und Grundwasserhaushalt Des Malmkarstes Im Süddeutschen Molassebecken, 1991, Bayerisches Landesamt für Wasserwirtschaft, Geologisches Landesamt Baden-Württemberg, München, Freiburg i.Br., 1990: p. 53.

[16] J. Birner, T. Fritzer, M. Jodocy, A. Savvatis, M. Schneider, I. Stober, Hydraulische Eigenschaften des Malmaquifers im Süddeutschen Molassebecken und ihre Bedeutung für die geothermische Erschließung., Z. Geol. Wiss. 40 (2012) 133–156.

[17] I. Stober, J. Birner, M. Wolfgramm, Hydrochemie der Tiefenwässer in Deutschland, Zeitschrift Für Geol. Wissenschaften. 41/42 (2014) 339.

[18] F. Heine, K. Zosseder, F. Einsiedl, Hydrochemical Zoning and Chemical Evolution of the Deep Upper Jurassic Thermal Groundwater Reservoir Using Water Chemical and Environmental Isotope Data, Water. 13 (2021) 1162. https://doi.org/10.3390/w13091162.

[19] M. Schneider, L. Thomas, Wissenschaftliche und technische Grundlagen zur strukturgeologischen und hydrogeologischen Charakterisierung tiefer geothermisch genutzter Grundwasserleiter am Beispiel des süddeutschen Molassebeckens, Berlin, 2012.

[20] H. Frisch, B. Huber, Ein Hydrogeologisches Modell und der Versuch einer Bilanzierung des Thermalwasservorkommens für den Malmkarst im Süddeutschen und im angrenzenden Oberösterreichischen Molassebecken, Hydrogeol. Und Umwelt. 20 (2000) 25–43.

[21] R.C. Capo, B.W. Stewart, O.A. Chadwick, Strontium isotopes as tracers of ecosystem processes: theory and methods, Geoderma. 82 (1998) 197–225. https://doi.org/10.1016/S0016-7061(97)00102-X.

[22] S. Santoni, F. Huneau, E. Garel, L. Aquilina, V. Vergnaud-Ayraud, T. Labasque, H. Celle-Jeanton, Strontium isotopes as tracers of water-rocks interactions, mixing processes and residence time indicator of groundwater within the granite-carbonate coastal aquifer of Bonifacio (Corsica, France), Sci. Total Environ. 573 (2016) 233–246. https://doi.org/10.1016/j.scitotenv.2016.08.087.

[23] K. Semhi, O. Abdalla, R. Al Abri, T. Al Hosni, I.D. Clark, Strontium isotopes as a tool for estimation of groundwater recharge and aquifer connectivity, Groundw. Sustain. Dev. 4 (2017) 1–11. https://doi.org/10.1016/j.gsd.2016.11.001.

[24] K.A. Baublys, S.K. Hamilton, H. Hofmann, S.D. Golding, A strontium (87Sr/86Sr) isotopic study on the chemical evolution and migration of groundwaters in a low-rank coal seam gas reservoir (Surat Basin, Australia), Appl. Geochemistry. 101 (2019) 1–18. https://doi.org/10.1016/j.apgeochem.2018.12.020.

[25] L. Bouchaou, N.R. Warner, T. Tagma, M. Hssaisoune, A. Vengosh, The origin of geothermal waters in Morocco: Multiple isotope tracers for delineating sources of water-rock interactions, Appl. Geochemistry. 84 (2017) 244–253. https://doi.org/10.1016/j.apgeochem.2017.07.004.

[26] L. Bouchaou, J.L. Michelot, A. Vengosh, Y. Hsissou, M. Qurtobi, C.B. Gaye, T.D. Bullen, G.M. Zuppi, Application of multiple isotopic and geochemical tracers for investigation of recharge, salinization, and residence time of water in the Souss–Massa aquifer, southwest of Morocco, J. Hydrol. 352 (2008) 267–287. https://doi.org/10.1016/j.jhydrol.2008.01.022.

[27] N. Ettayfi, L. Bouchaou, J.L. Michelot, T. Tagma, N. Warner, S. Boutaleb, M. Massault, Z. Lgourna, A. Vengosh, Geochemical and isotopic (oxygen, hydrogen, carbon, strontium) constraints for the origin, salinity, and residence time of groundwater from a carbonate aquifer in the Western Anti-Atlas Mountains, Morocco, J. Hydrol. 438–439 (2012) 97–111. https://doi.org/10.1016/j.jhydrol.2012.03.003.

[28] A. Probst, A. El Gh'mari, D. Aubert, B. Fritz, R. McNutt, Strontium as a tracer of weathering processes in a silicate catchment polluted by acid atmospheric inputs, Strengbach, France, Chem. Geol. 170 (2000) 203–219. https://doi.org/10.1016/S0009-2541(99)00248-X.

[29] W.H. Burke, R.E. Denison, E.A. Hetherington, R.B. Koepnick, H.F. Nelson, J.B. Otto, Variation of seawater 87Sr/86Sr throughout Phanerozoic time, Geology. 10 (1982) 516. https://doi.org/10.1130/0091-7613(1982)10<516:VOSSTP>2.0.CO;2.

[30] P.C. Smalley, A.C. Higgins, R.J. Howarth, H. Nicholson, C.E. Jones, N.H.M. Swinburne, J. Bessa, Seawater Sr isotope variations through time: A procedure for constructing a reference curve to date and correlate marine sedimentary rocks, Geology. 22 (1994) 431. https://doi.org/10.1130/0091-7613(1994)022<0431:SSIVTT>2.3.CO;2.

[31] J. Veizer, W. Compston, 87Sr/86Sr composition of seawater during the Phanerozoic, Geochim. Cosmochim. Acta. 38 (1974) 1461–1484. https://doi.org/10.1016/0016-7037(74)90099-4.

[32] J. Schneider, Ergebnisse der hydrochemischen und isotopenhydrologischen Untersuchungen während der Airlifttests an der Bohrung TR-GT1 im Geothermieprojekt Traunreut, Hydrosion GmbH, unveröffentl., München, 2013.

[33] Interreg-IIIA, Grenzüberschreitende Bewirtschaftung des Grundwassers im Raum Hegau – Schaffhausen, 2008.

[34] J. Veizer, D. Ala, K. Azmy, P. Bruckschen, D. Buhl, F. Bruhn, G. a. F. Carden, A. Diener, S. Ebneth, Y. Godderis, T. Jasper, C. Korte, F. Pawellek, O.G. Podlaha, H. Strauss, 87Sr/86Sr, δ13C and δ18O evolution of Phanerozoic seawater, Chem. Geol. 161 (1999) 59–88. https://doi.org/10.1016/S0009-2541(99)00081-9.

[35] H.N. Waber, M. Heidinger, G. Lorenz, D. Traber, Arbeitsbericht NAB 13-63: Hydrochemie und Isotopenhydrogeologie von Tiefengrundwässern in der Nordschweiz und im angrenzenden Süddeutschland, Wettingen, 2014.

[36] K. Thuro, K. Zosseder, D. Bohnsack, F. Heine, F. Konrad, E. Mraz, G. Stockinger, Dolomitkluft: Erschließung, Test und Analyse des ersten kluftdominierten Dolomitaquifers im tiefen Malm des Molassebeckens zur Erhöhung der Erfolgsaussichten, Munich, Germany, 2019.

[37] N.G. Hemming, G.N. Hanson, Boron isotopic composition and concentration in modern marine carbonates, Geochim. Cosmochim. Acta. 56 (1992) 537–543. https://doi.org/10.1016/0016-7037(92)90151-8.

[38] E. Dotsika, D. Poutoukis, J.L. Michelot, W. Kloppmann, Stable Isotope and Chloride, Boron Study for Tracing Sources of Boron Contamination in Groundwater: Boron Contents in Fresh and Thermal Water in Different Areas in Greece, Water. Air. Soil Pollut. 174 (2006) 19–32. https://doi.org/10.1007/s11270-005-9015-8.

[39] H. Marschall, G. Foster, Advances in Isotope Geochemistry: Boron Isotopes The Fifth Element, 2018. https://doi.org/https://doi.org/10.1007/978-3-319-64666-4.

[40] F. Heine, A. Peña, K. Zosseder, F. Einsiedl, Schlussbericht: IsoMol - Analytik - Hydro- und Isotopenchemie in der Bayerischen Molasse, München, 2018.

[41] E. Mraz, M. Wolfgramm, I. Moeck, K. Thuro, Detailed Fluid Inclusion and Stable Isotope Analysis on Deep Carbonates from the North Alpine Foreland Basin to Constrain Paleofluid Evolution, Geofluids. 2019 (2019) 1–23. https://doi.org/10.1155/2019/8980794.

[42] J. Véron, The Alpine Molasse Basin: review of petroleum geology and remaining potential, Bull. Angew. Geol. 10 (2005) 75–86. https://doi.org/10.5169/seals-225567.

[43] W. Freudenberger, K. Schwerd, Erläuterungen zur Geologischen Karte von Bayern 1:500000, 4th ed., Bayerisches Geologisches Landesamt, Munich, 1996.

[44] F. Heine, F. Einsiedl, Groundwater dating with dissolved organic radiocarbon: A promising approach in carbonate aquifers, Appl. Geochemistry. 125 (2021) 1–13. https://doi.org/10.1016/j.apgeochem.2020.104827.

[45] W. Liedmann, Diagenetische Entwicklung Süddeutscher Malmkarbonate, Universität Heidelberg, 1992.

[46] E. Villinger, Bemerkungen zur Verkarstung des Malms unter dem westlichen süddeutschen Molassebecken, Bull. Ver. Schweiz. Pet. u. -Ing. 54 (1988) 41–59. https://doi.org/10.5169/seals-211748.

[47] C. Reinhold, Prozesse, Steuerung und Produkte komplexer Diagenese-Sequenzen in süddeutschen Malm-Karbonaten, Technische Universität Berlin, 1996.

[48] G.H. Bachmann, M. Müller, K. Weggen, Evolution of the Molasse Basin (Germany, Switzerland), Tectonophysics. 137 (1987) 77–92. https://doi.org/10.1016/0040-1951(87)90315-5.

[49] K. Lemcke, Geologie von Bayern I. - Das bayerische Alpenvorland vor der Eiszeit - Erdgeschichte - Bau - Bodenschätze, Schweizerbart, Stuttgart, 1988.

[50] E. Mraz, Reservoir Characterization to Improve Exploration Concepts of the Upper Jurassic in the Southern Bavarian Molasse Basin, Technical University of Munich, 2019.

[51] R.K.F. Meyer, H. Schmidt-Kaler, Paläogeographischer Atlas des süddeutschen Oberjura (Malm), Geol. Jahrb. 115 (1989) 3–77.

[52] R.K.E. Meyer, H. Schmidt-Kaler, Paläogeographie und Schwammriffentwicklung des süddeutschen Malm - ein Überblick, Facies. 23 (1990) 175–184.

[53] D. Bohnsack, M. Potten, S. Freitag, F. Einsiedl, K. Zosseder, Stress sensitivity of porosity and permeability under varying hydrostatic stress conditions for different carbonate rock types of the geothermal Malm reservoir in Southern Germany, Geotherm. Energy. (2021). https://doi.org/10.1186/s40517-021-00197-w.

[54] D. Bohnsack, M. Potten, D. Pfrang, P. Wolpert, K. Zosseder, Porosity–permeability relationship derived from Upper Jurassic carbonate rock cores to assess the regional hydraulic matrix properties of the Malm reservoir in the South German Molasse Basin, Geotherm. Energy. 8 (2020) 47. https://doi.org/10.1186/s40517-020-00166-9.

[55] F. Konrad, A. Savvatis, F. Wellmann, K. Zosseder, Hydraulic behavior of fault zones in pump tests of geothermal wells: a parametric analysis using numerical simulations for the Upper Jurassic aquifer of the North Alpine Foreland Basin, Geotherm. Energy. 7 (2019) 25. https://doi.org/10.1186/s40517-019-0137-4.

[56] F. Konrad, A. Savvatis, D. Degen, F. Wellmann, F. Einsiedl, K. Zosseder, Productivity enhancement of geothermal wells through fault zones: Efficient numerical evaluation of a parameter space for the Upper Jurassic aquifer of the North Alpine Foreland Basin, Geothermics. 95 (2021) 102119. https://doi.org/10.1016/j.geothermics.2021.102119.

[57] F. Böhm, A. Savvatis, U. Steiner, M. Schneider, R. Koch, Lithofazielle Reservoircharakterisierung zur geothermischen Nutzung des Malm im Großraum München. [Lithofacies and characterization of the geothermal Malm reservoir in the greater area of Munich], Grundwasser. 18 (2013) 3–13. https://doi.org/10.1007/s00767-012-0202-4.

[58] A. Savvatis, U. Steiner, B. Huber, T. Fritzer, M. Schneider, Limitierungen bei der Ermittlung der Grundwasserfließrichtung in tiefen Aquiferen am Beispiel des Malms im Süddeutschen Molassebecken, Grundwasser. 20 (2015) 271–280. https://doi.org/10.1007/s00767-015-0304-x.

[59] B. Wagner, G. Kus, B. Kainzmauer, T. Spörlein, T. Wilferth, W. Veit, P. Fritsch, M. Wrobel, W. Lindenthal, J. Neumann, W. Sprenger, Erläuterungen zur Hydrogeologischen Karte von Bayern, Bayerisches Landesamt für Umwelt, Augsburg, 2009.

[60] M. Heidinger, F. Eichinger, R. Purtschert, P. Mueller, J. Zappala, G. Wirsing, T. Geyer, T. Fritzer, D. Groß, Altersbestimmung an thermalen Tiefenwässern im Oberjura des Molassebeckens mittels Krypton-Isotopen, Grundwasser. 24 (2019) 287–294. https://doi.org/10.1007/s00767-019-00431-0.

[61] B. Bertleff, Das Strömungssystem der Grundwässer im Malm-Karst des West-Teils des süddeutschen

Molassebeckens, Abh. geol. Landesamt Baden-Württemberg, 1986.

[62] S. Geyer, M. Wolf, L.I. Wassenaar, P. Fritz, G. Buckau, J.I. Kim, Isotope investigations on fractions of dissolved organic carbon for 14C groundwater dating, in: Int. At. Energy Agency, International Atomic Energy Agency, Vienna, Austria, 1993: pp. 359–380.

[63] B. Huber, Das Thermalwasservorkommen im niederbayerisch-oberösterreichischen Molassebecken, München, 1999.

[64] J.E. Goldbrunner, Zum Stand der geothermischen und balneologischen Tiefengrundwassernutzung im Oststeirischen Becken und im Oberösterreichischen Molassebecken, Z. Dt. Geol. Ges. 138 (1987) 513–526.

[65] J.N. Andrews, M.J. Youngman, J.E. Goldbrunner, W.G. Darling, The geochemistry of formation waters in the molasse basin of upper Austria, Environ. Geol. Water Sci. 10 (1987) 43–57. https://doi.org/10.1007/BF02588004.

[66] R.K.F. Meyer, Moosburg 4, die erste Kernbohrung durch den Malm unter der bayerischen Molasse, Erlanger Geol. Abh. 123 (1994) 51–81.

[67] G. Faure, J.L. Powell, Strontium Isotope Geology, in: W. von Engelhardt, T. Hahn, R. Roy, P.J. Wyllie (Eds.), Miner. Rocks Inorg. Mater., Springer Berlin Heidelberg, Berlin, Heidelberg, New-York, 1972: p. 188. https://doi.org/10.1007/978-3-642-65367-4.

[68] A. Vengosh, Y. Kolodny, A. Starinsky, A.R. Chivas, M.T. McCulloch, Coprecipitation and isotopic fractionation of boron in modern biogenic carbonates, Geochim. Cosmochim. Acta. 55 (1991) 2901–2910. https://doi.org/10.1016/0016-7037(91)90455-E.

[69] DIN EN 13657:2003-01, Characterization of waste - Digestion for subsequent determination of aqua regia soluble portion of elements in waste, 2003.

[70] DIN EN ISO 11885:2009-09, Water quality - Determination of selected elements by inductively coupled plasma optical emission spectrometry (ICP-OES) (ISO 11885:2007), 2019.

[71] DIN EN ISO 17294-2:2017-01, Water quality - Application of inductively coupled plasma mass spectrometry (ICP-MS) - Part 2: Determination of selected elements including uranium isotopes (ISO 17294-2:2016), 2017.

[72] A.A. Baba, A.O. Omipidan, F.A. Adekola, O. Job, A.G.F. Alabi, A. Baral, R. Samal, Optimization study of a nigerian dolomite ore dissolution by hydrochloric acid, J. Chem. Technol. Metall. 49 (2014) 280–287.

[73] J. Mahlknecht, D. Merchán, M. Rosner, A. Meixner, R. Ledesma-Ruiz, Assessing seawater intrusion in an arid coastal aquifer under high anthropogenic influence using major constituents, Sr and B isotopes in groundwater, Sci. Total Environ. 587–588 (2017) 282–295. https://doi.org/10.1016/j.scitotenv.2017.02.137.

[74] M. Rosner, Geochemical and instrumental fundamentals for accurate and precise strontium isotope data of food samples: Comment on "Determination of the strontium isotope ratio by ICP-MS ginseng as a tracer of regional origin" (Choi et al., 2008), Food Chem. 121 (2010) 918–921. https://doi.org/10.1016/j.foodchem.2010.01.019.

[75] M. Rosner, W. Pritzkow, J. Vogl, S. Voerkelius, Development and validation of a method to determine the boron isotopic composition of crop plants, Anal. Chem. 83 (2011) 2562–2568. https://doi.org/10.1021/ac102836h.

[76] J. Gaillardet, D. Lemarchand, C. Göpel, G. Manhès, Evaporation and sublimation of boric acid: Application for boron purification from organic rich solutions, Geostand. Newsl. 25 (2001) 67–75. https://doi.org/10.1111/j.1751-908X.2001.tb00788.x.

[77] R. Gonfiantini, S. Tonarini, M. Gröning, A. Adorni-Braccesi, A.S. Al-Ammar, M. Astner, S. Bächler, R.M. Barnes, R.L. Bassett, A. Cocherie, A. Deyhle, A. Dini, G. Ferrara, J. Gaillardet, J. Grimm, C. Guerrot, U. Krähenbühl, G. Layne, D. Lemarchand, A. Meixner, D.J. Northington, M. Pennisi, E. Reitznerová, I. Rodushkin, N. Sugiura, R. Surberg, S. Tonn, M. Wiedenbeck, S. Wunderli, Y. Xiao, T. Zack, Intercomparison of Boron Isotope and Concentration Measurements. Part II: Evaluation of Results, Geostand. Geoanalytical Res. 27 (2003) 41–57.

https://doi.org/10.1111/j.1751-908X.2003.tb00711.x.

[78] R.B. Koepnick, R.E. Denison, W.H. Burke, E.A. Hetherington, D.A. Dahl, Construction of the Triassic and Jurassic portion of the Phanerozoic curve of seawater 87Sr/86Sr, Chem. Geol. Isot. Geosci. Sect. 80 (1990) 327–349. https://doi.org/10.1016/0168-9622(90)90014-4.

[79] J.M. McArthur, R.J. Howarth, G.A. Shields, Strontium Isotope Stratigraphy, in: F.M. Gradstein, J.G. Ogg, M.D. Schmitz, G.M. Ogg (Eds.), Geol. Time Scale, Elsevier, 2012: pp. 127–144. https://doi.org/10.1016/B978-0-444-59425-9.00007-X.

[80] B. Wagner, Bayerisches Landesamt für Lithogeochemische Hintergrundwerte der Gesteine Bayerns, 2020.

[81] X. Wang, Z. Tang, X. Dong, Distribution of strontium isotopes in river waters across the tarim basin: A map for migration studies, J. Geol. Soc. London. 175 (2018) 967–973. https://doi.org/10.1144/jgs2018-074.

[82] P. Fritz, Zur Genese von Dolomiten und zuckerkörnigem Kalk im Weißen Jura der Schwäbischen Alb (Württemberg), 1966.

[83] H.B. Lang, Dolomit und zuckerkörniger Kalk im Weißen Jura der mittleren Schwäbischen Alb (Württemberg), N. b. Geol. Abh. 120 (1964) 253–299.

[84] N.G. Hemming, R.J. Reeder, G.N. Hanson, Mineral-fluid partitioning and isotopic fractionation of boron in synthetic calcium carbonate, Geochim. Cosmochim. Acta. 59 (1995) 371–379. https://doi.org/10.1016/0016-7037(95)00288-B.

[85] K. Klochko, A.J. Kaufman, W. Yao, R.H. Byrne, J.A. Tossell, Experimental measurement of boron isotope fractionation in seawater, Earth Planet. Sci. Lett. 248 (2006) 276–285. https://doi.org/10.1016/j.epsl.2006.05.034.

[86] S.-Y. Jiang, M.R. Palmer, Boron isotope systematics of tourmaline from granites and pegmatites: a synthesis, Eur. J. Mineral. 10 (1998) 1253–1266. https://doi.org/10.1127/ejm/10/6/1253.

[87] R. van Geldern, A. Baier, H.L. Subert, S. Kowol, L. Balk, J.A.C. Barth, Pleistocene paleo-groundwater as a pristine fresh water resource in southern Germany – evidence from stable and radiogenic isotopes, Sci. Total Environ. 496 (2014) 107–115. https://doi.org/10.1016/j.scitotenv.2014.07.011.

[88] R. Hänel, M. Kleefeldt, I. Koppe, Geothermisches Energiepotential. Pilotstudie: Abschätzung der geothermischen Energievorräte an ausgewählten Beispielen in der Bundesrepublik Deutschland, Hannover, 1984.

[89] W. Stichler, Isotopengehalte in Tiefengrundwässern aus Erdöl- und Erdgasbohrungen im süddeutschen Molassebecken, Beiträge Zur Hydrogeol. 48 (1997) 81–88.

[90] Y.K. Kharaka, J.S. Hanor, Deep Fluids in Sedimentary Basins, in: H.D. Holland, K.K. Turekian (Eds.), Treatise on Geochemistry, Elsevier, 2014: pp. 471–515. https://doi.org/10.1016/B978-0-08-095975-7.00516-7.

[91] H. Furtak, H. Langguth, Zur hydrochemischen Kennzeichnung von Grundwässern und Grundwassertypen mittels Kennzahlen, Mem. IAH-Congress. VII (1967) 86–96.

[92] J. Pu, D. Yuan, C. Zhang, H. Zhao, Tracing the sources of strontium in karst groundwater in Chongqing, China: a combined hydrogeochemical approach and strontium isotope, Environ. Earth Sci. 67 (2012) 2371–2381. https://doi.org/10.1007/s12665-012-1683-2.

[93] J.C. Pett-Ridge, L.A. Derry, J.K. Barrows, Ca/Sr and 87Sr/86Sr ratios as tracers of Ca and Sr cycling in the Rio Icacos watershed, Luquillo Mountains, Puerto Rico, Chem. Geol. 267 (2009) 32–45. https://doi.org/10.1016/j.chemgeo.2008.11.022.

[94] P. Shand, D.P.F. Darbyshire, A.J. Love, W.M. Edmunds, Sr isotopes in natural waters: Applications to source characterisation and water–rock interaction in contrasting landscapes, Appl. Geochemistry. 24 (2009) 574–586. https://doi.org/10.1016/j.apgeochem.2008.12.011.

[95] T. Tütken, T.W. Vennemann, H. Janz, E.P.J. Heizmann, Palaeoenvironment and palaeoclimate of the Middle Miocene lake in the Steinheim basin, SW Germany: A reconstruction from C, O, and Sr isotopes of fossil remains, Palaeogeogr. Palaeoclimatol. Palaeoecol. 241 (2006) 457–491. https://doi.org/10.1016/j.palaeo.2006.04.007.

[96] W. Ufrecht, S. Hölzl, Salinare Mineral- und Thermalwässer im Oberen Muschelkalk (Trias) im Großraum Stuttgart – Rückschlüsse auf Herkunft und Entstehung mit Hilfe der 87Sr/86Sr-Strontium-Isotopie, Zeitschrift Der Dtsch. Gesellschaft Für Geowissenschaften. 157 (2006) 299–315. https://doi.org/10.1127/1860-1804/2006/0157-0299.

[97] B. Köhl, M. Elsner, T. Baumann, Hydrochemical and operational parameters driving carbonate scale kinetics at geothermal facilities in the Bavarian Molasse Basin, Geotherm. Energy. 8 (2020) 26. https://doi.org/10.1186/s40517-020-00180-x.

[98] H.J. Unger, Die Bohrungen Köfering und Schierling 1 südlich Regensburg und ihr geologisch-tektonischer Rahmen, in: Geol. Jahrb. R. A, Bundesanstalt für Geowissenschaften und Rohstoffe und die Geologischen Landesämter der Bundesrepublik Deutschland, Hannover, 1987: pp. 57–74.

[99] S. Barth, Boron isotope variations in nature: a synthesis, Geol. Rundschau. 82 (1993) 640–651. https://doi.org/10.1007/BF00191491.